ELECTRICAL, OPTICAL AND STRUCTUAL PROPERTIES IN ELECTROCHROMIC WO_3 FILMS

by

Jianping Zhang

B.Sc. (Honours) **Zhongshan University**, 1982

THESIS SUBMITTED IN PARTIAL FULFILLMENT OF
THE REQUIREMENTS FOR THE DEGREE OF
MASTER OF SCIENCE

in the Department
of
Physics

SIMON FRASER UNIVERSITY

May, 1989

APPROVAL

Name: Jianping Zhang

Degree: Master of Science

Title of Thesis: Electrical, Optical and Structural Properties in Electrochromic WO_3 Films

Examining Committee:

Chairman: Dr. E. D. Crozier

Dr. K. Colbow
Senior Supervisor

Dr. R. F. Frindt

Dr. S. R. Morrison

Dr. M. L. W. Thewalt
Examiner
Professor, Physics, SFU

Date Approved May 4, 1989

PARTIAL COPYRIGHT LICENSE

I hereby grant to Simon Fraser University the right to lend my thesis, project or extended essay (the title of which is shown below) to users of the Simon Fraser University Library, and to make partial or single copies only for such users or in response to a request from the library of any other university, or other educational institution, on its own behalf or for one of its users. I further agree that permission for multiple copying of this work for scholarly purposes may be granted by me or the Dean of Graduate Studies. It is understood that copying or publication of this work for financial gain shall not be allowed without my written permission.

Title of Thesis/Project/Extended Essay

Electrical, Optical and Structural Properties in Electrochromic WO_3 Films

Author:

(signature)

Jianping Zhang

(name)

May 30, 1989

(date)

ABSTRACT

Electrochromic tungsten trioxide films of 200 to 650±20 nm thickness were deposited onto glass slides and SnO_2:F substrates using spray pyrolysis. The investigations of electrochemically colored WO_3 films revealed large variations in electrical, optical and structural properties during the electrochromic process.

The resistivity and the carrier concentration of electrochromic WO_3 films were obtained by Van der Pauw's technique. The resistivities of as-prepared WO_3 films deposited onto glass at substrate temperatures between 200°C and 400°C were found to be in the range of $10^5 - 1$ Ω·cm and decreased by 2 to 8 orders of magnitude after coloration. The carrier concentration of the colored films was estimated to be about 10^{21} cm^{-3}.

X-ray diffraction studies revealed structural changes in the polycrystalline WO_3 films deposited at substrate temperatures greater than 300°C during the electrochromic process. The X-ray diffraction peaks for colored films could be assigned to hydrogen tungsten bronze (H_xWO_3); the structure of the bleached films reverted to the original uncolored state (WO_3).

The reflectance properties of colored polycrystalline WO_3 films can be predicted theoretically by the free electron Drude theory. Measurements of infrared reflectances showed that the polycrystalline WO_3 films deposited at a higher temperature have higher infrared reflectivity. The electrons injected into such films likely show free electron behavior.

Dedicated to my parents and my wife
for their continual support and encouragement

Acknowledgements

I wish to express my sincere thanks to my senior supervisor, Dr. K. Colbow, for his encouragement and financial support during the course of this research. Thanks also to Dr. R. F. Frindt and Dr. S. R. Morrison for acting as the members of my supervisor committee and examining committee, and to Dr. M. L. W. Thewall for being my examiner. Their valuable comments and suggestions were a great help to improving the original version of this thesis.

My special thanks go to Dr. S. Wessel for her concrete guidance and helpful discussions and for her kindness in correcting the hand written manuscript of my thesis. I sincerely thank M. Nissen who spent many hours in IR reflectance measurements for me. I would like to thank the staff, faculty and fellow graduate students of the Physics Department for their concern and help with various aspects of this work.

Finally, the Graduate Fellowship from SFU and the TA'ships from the Physics Department of SFU are also very appreciated.

TABEL OF CONTENTS

List of Tables

List of Figures

Chapter 1

INTRODUCTION

The interest in research on electrochromic materials in recent years arises from the development of electrochromic window applications for efficient solar energy control[1-3] and display devices[4]. Many investigations have been carried out on the mechanism of electrochromism associated with variations in optical, electrical, thermodynamic and structural properties during the electrochromic process.

Electrochromism is exhibited by a number of materials: both inorganic and organic liquids and solids. The major research published to date concerns transition-metal oxides, such as WO_3, MoO_3, Ir_2O_3, V_2O_5 and doped $SrTiO_3$[5]. Several organic materials, such as viologen, pyrazoline and conductive organic polymers, also exhibit electrochromism. Among these electrochromic materials, tungsten trioxide (WO_3) is the most promising material and is therefore widely studied.

1.1 Preparation Techniques and Physical Properties of WO_3 Films

Tungsten trioxide films can be prepared by various deposition

techniques, such as vacuum evaporation[6–8], rf sputtering[9–12], chemical vapor deposition(CVD)[13] and spray pyrolysis[14].

The physical and structural properties of the deposited oxide films depend largely on the preparation conditions, such as the substrate temperature[6], the crystallinity of the substrate[14] and the pressure of atmosphere or carrier gas flow rate[9].

The most frequently used preparation technique for WO_3 films is vacuum evaporation[6–8]. Miyake *et al.*[6] found that the films evaporated at a substrate temperature lower than 350℃ are amorphous in structure with a resistivity of $10^9 - 10^5$ Ω·cm, while films evaporated at the substrate temperature higher than 400°C are mainly crystalline in nature with a resistivity of $10^2 - 10^{-3}$ Ω·cm. The authors reported that the resistivity decreases from 10^9 to 10^{-3} Ω·cm with increasing deposition temperature from 200° C to 500° C and is almost constant ($1.5 \cdot 10^9$ Ω·cm) for the temperature range of 50 – 200℃.

It was also found that evaporated amorphous WO_3 films crystallized when the films were annealed thermally for several hours in air or N_2 gas at temperatures larger than 300℃[8,12,15,16]. Nakamara[16] investigated the dependence of the optical properties of WO_3 films on annealing temperature, and found that the optical gap decreases with increasing annealing temperature up to 250°C. Annealing at 300℃ leads to a change in the shape of the absorption spectrum which was associated with increased crystallinity of the films.

Another frequently used deposition technique is rf sputtering[9–12]. Cogan *et al.*[10] found that the crystallinity of rf sputtered films was controlled by varying the substrate temperature during deposition, and that films have a crystalline structure at deposition temperature over 150°C. Kaneko *et al.*[9] investigated the physical properties, such as the dependence of the resistivity of rf sputtered films on the oxygen concentration of Ar/O_2 gas mixtures and the total operating pressure. They found that the electrical resistivity of WO_3 films increases considerably with increasing O_2 concentration from 0.5 – 50% in Ar/O_2 and with increasing total sputtering pressure in the range of $0.5 - 6 \cdot 10^{-2}$ Torr. Kaneko *et al.*[9] found that not only the substrate temperature but also the oxygen concentration of the Ar/O_2 mixture and the operating pressure are also major factors which determine the crystallinity of rf sputtered films.

A pyrolytic spray deposition technique was reported by Craigen *et al.*[14] in 1986. The WO_3 films prepared pyrolytically from a solution containing WCl_6 and N,N-Dimethyl Formamide have similar electrochromic properties as films prepared by other methods[6,9]. However, this method has the advantage that it is simple and inexpensive, and has the potential for the production of large area electrochromic devices with low capital and production costs.

Other WO_3 film deposition techniques, such as chemical vapor deposition and electrolytic precipitation, have been tried recently[13].

1.2 Structure of Tungsten Trioxide

In order to understand the physical and structural properties of WO_3 material, many authors have investigated it by various methods [17-21]. Tanisaki[18], Salje and Viswanathan[19] investigated the crystal structure at different temperatures and found that the pure WO_3 single crystals exhibit at least five different phases in the temperature range of 900°C to –155°C, changing through the sequence of tetragonal – orthorhombic – monoclinic – triclinic – monoclinic structures during cooling. Tanisaki[18] reported that the crystal structure of WO_3 is monoclinic at room temperature (27°C), it transforms to a triclinic structure near 17°C and to monoclinic structure near –40°C. They also found that the dependence of resistivity on temperature has a weak anomaly at 17°C and a stronger anomaly at –40°C. These discontinuities were associated with corresponding phase transitions. Salje *et al.*[19] studied the phase transitions in WO_3 crystals by Raman and absorption spectroscopies. They observed two stable (or metastable) states of the crystals at room temperature; one monoclinic WO_3(I), and the other triclinic WO_3(II). The tungsten trioxide became orthorhombic above 330°C and tetragonal above 740°C. They also reported that WO_3 is an insulator at low temperatures and a semiconductor at high temperatures.

The crystal structure of WO_3 films, which depends on the deposition techniques and preparation conditions as described in 1.1, was found mainly to be monoclinic at room temperature[6,22]. Figure 1.1 shows the crystal structure of WO_3 with cubic approximation based on corner-sharing

of WO_6 octahedrons. However, structural analyses of WO_3 have revealed considerable deviation from the ideal cubic perovskite type. The distortion was ascribed to antiferroelectric displacements of W atoms and mutual rotations of oxygen octahedrons. The type and magnitude of the distortions were found to be dependent on temperature[23]. Figure 1.2 illustrates the distortion in the monoclinic structure; the W–O bonds form zigzag chains along the three crystallo graphic axes with W–O–W angles of 158 ± 2.3^0 and O–W–O angles of 166 ± 5.6^0[23]. In the **a** direction the bonds were found to be approximately 1.9Å while in the **b** and **c** directions the W–O bonds are alternately long (2.1Å) and short (1.7Å)[23]. For the orthorhombic symmetry, the deviation from the ideal perovskite structure is characterized by a zigzag motion of the W position in the **b** and **c** directions as well as a tilt system with tilt angles around **a**[20].

The structure of thin amorphous WO_3 films has been investigated by Zeller[17] in 1977. The author suggested that amorphous WO_3 is built up of a disordered network of corner sharing octahedrons. The disordered network not only contains four membered rings but also three, five and six membered species[17]. Recently, Gabrusenoks *et al.*[21] investigated amorphous films by Raman scattering spectroscopy, and proposed that WO_3 is composed of a spatial network of tightly bound $(WO_6)_n \cdot mH_2O$ clusters with a large number of terminal oxygen W=O and W–O–W bonds between clusters. The clusters with dimensions no larger than 20–30Å are built from 3–8 WO_6 octahedrons, linked together by corners or edges in such a manner as to guarantee the porous structure of amorphous WO_3 film. The voids observed within the film are the result of random packing of the clusters and mostly give an open structure which is normally filled

with molecular water taken from the air. This latter model is considered to be more realistic than the disordered network model of the corner-sharing octahedrons[17].

The molecular water present in amorphous WO_3 films strongly affects physical and structural properties. However, experiments showed that H_2O can be removed by heating the films[16]. Nakamura[16] found two kinds of absorption peaks in the infrared region for evaporated amorphous films, one is a broad absorption band located at 2.7 μm and is assigned to the O–H stretching vibration; the other is observed at 6.2 μm and is assigned to O–H–O deformation vibration. The magnitude of these absorption bands can be reduced substantially after annealing. Thus this phenomena is believed to be related to the escape of water from the inside of the films[16].

1.3 Electrochromism of WO_3 Films

WO_3 films can be colored electrochromically in various ways. Deb[8] in 1973 first discovered the electrochromic effect by applying a large DC electrical field of 10^4 V/cm across an evaporated WO_3 film at room temperature. The coloration was observed originating at the cathode and propagating slowly towards the anode. Using this method, the coloration process requires several hours depending on the presence of moisture[8]. Later, Zeller[17] carried out similar experiments under controlled humidity conditions, and observed quantitatively the propagation speed and intensity of the color front as a function of relative humidity.

WO_3 films were also colored by an electrochemical process[24]. WO_3 films deposited onto a transparent conductive SnO_2-coated glass slide were used as the negative electrode and Pt wire as the positive electrode. Both electrodes were inserted into an electrolyte, such as H_2SO_4 in H_2O or $LiClO_4$ in an organic solvent[24]. Then, a small voltage (0.5 V) was applied across the electrodes, the film turned blue immediately. By removing the voltage source, i.e. in open circuit condition, the films remained colored. However the films may be bleached by shorting the electrodes or reversing the polarity.

Another experiment to color WO_3 films was done by Crandall *et al.*[25]. The authors covered a limited region of a WO_3 film surface with an aqueous electrolyte containing 20% H_2SO_4. In the center of the electrolyte, an indium wire touched the WO_3 film. Coloration appeared around the tip and then diffused radially outward from the indium source.

In order to establish dynamic control properties for the purpose of display devices, a standard electrochromic cell (EC cell) was created[1,5]. Figure 1.3 shows the sandwich structure of an EC cell. Generally, it consists of several materials: two transparent conducting layers, an ion conductor, an ion storage layer and the electrochromic material WO_3. The WO_3 film on the conducting layer is used as working electrode (WE) and another conducting layer is used as counter electrode (CE). The transparent conducting layer should be as transparent as possible and highly conductive to minimize current loss and heating of the window, such as films of the doped oxide semiconductors In_2O_3:Sn, SnO_2:F, SnO_2:Sb or Cd_2SnO_4. Ion storage provides ions which inject into or withdraw from, the

electrochromic layer in the electrochromic reaction via the ion conductor. The detailed design can be a liquid electrolyte device or solid electrolyte device. For devices using liquid electrolytes, the electrolyte can serve as both storage and conductor for the ions, while in an all-solid state device the ion conductor can be an appropriate dielectric material and the ion storage can be an electrochromic layer. One may also combine the conductor and storage media into one layer[1]. EC cells operate at the colored state by applying a small voltage with the negative polarity to the working electrode, and return to the uncolored state by reversing the bias of the electrode.

1.3.1 Mechanism of Electrochromism

Since the electrochromism in WO_3 films was discovered, many investigations have been carried out to understand the mechanism of electrochromism, and various models have been suggested. These models are based on the different experiments and coloring conditions.

Deb[8] used a color center mechanism to explain WO_3 films being colored by applying a large electrical field. In the presence of the electrical field, the electrons injected into the conduction band are captured by positively charged structural defects such as anion vacancies. The electrons held by the coulombic field of vacancies will be essentially similar to F-centers in other ionic solids. The excited state of the F-center is assumed to be located below the conduction band.

In 1975, Chang *et al.*[26] suggested an oxygen extraction model based on the electrochemichromic system. They ascribed the blue color in WO_3 film to an electrochemical reaction in the form by the following equation:

$$mWO_3 + 2nH^+ + 2ne^- \longrightarrow W_mO_{3m-n}(blue) + nH_2O \qquad (1.1)$$

In the same year, Hurditch[27] studied electrochromism in WO_3 films containing H_2O, such as evaporated or chemically prepared amorphous films, and proposed a similar and more complex model in which the electrocoloration process is attributed to the formation of a "tungsten-blue" phase following cathodic reduction by active hydrogen:

$$WO_3 \cdot aq + mH \longrightarrow WO_{3-m}(OH)_m \cdot aq \qquad (1.2)$$

The active hydrogen atoms are generated by reduction of H^+ at the cathode, and the H^+ ions are dissociated from some fraction of the H_2O molecules in the film.

Another model proposed by Faughnan *et al.*[28,29] is the double injection model. In this model, the coloration of the WO_3 film was achieved by simultaneous injection of electrons and cations into interstitial sites in the WO_3 lattice thereby forming a tungsten bronze (M_xWO_3) according to

$$WO_3 + xe^- + xM^+ \longrightarrow M_xWO_3 \qquad (1.3)$$

where M^+ is a positive ion, such as proton (H^+), and x is a parameter with $o<x<1$ which is a measure of both the electron and cation concentration injected into the film.

In 1977, Schirmer *et al.*[15] suggested a model closely related to the double injection model. The authors attributed the coloration due to the a broad absorption band which can be explained as the optical absorption of small polarons. A small polaron is formed if the interation of a charge carrier with the surrounding lattice localizes the carrier to one lattice site[15].

Although various models were suggested, the mechanism of electrochromism in WO_3 is still not completely understood. All models suggested above are supported only by some experimental results and ruled out by others.

Hersh *et al.*[24] found by X-ray photoelectron spectra (XPS) no change in the W–O ratio after coloration, therefore O^{2-} was not extracted to form WO_{3-x}. This evidence works against the oxygen extraction model. The authors also argued against an F-center mechanism since the color center densities are estimated to be on the order of 10^{21} cm^{-3} by measurement of current density, while typical densities of F-centers are only 10^{17} cm^{-3}. However, they proved by XPS that ions and electrons are involved in the coloration mechanism and that the film does not color in the absence of cations. Thus the experiments provided evidence for the double injection model of electrochromism with the formation of tungsten bronze.

The broad absorption band peaked at energies near 1.2 – 1.5 eV for amorphous films and 0.84 eV for crystalline films[8,15,28] can be explained by the double injection model. According to this model, the electrons entering WO_3 layers from the cathode are distributed throughout the WO_3 lattice and accommodated in W^{5+} 5d orbitals. The optical absorption arises from the intervalence transitions, i.e. an electron located at one W ion is excited over a barrier to be trapped at another W ion site without phonon emission. The transition can be written as[28]:

$$W^{5+}(A) + W^{6+}(B) + h\upsilon \longrightarrow W^{6+}(A) + W^{5+}(B) \qquad (1.4)$$

where A and B refer to the two different W ion sites. Schirmer *et al.*[15] pointed out that since all tungsten sites are not equivalent in the amorphous material, the injected electrons will be preferentially trapped at deeper sites than in the polycrystalline material. This variation in trap depths will add an additional term E_0 in the energy of the transition[29]. This result explains why the optical absorption shifts to lower energy in crystalline WO_3, typically from 1.4 eV in the amorphous state to 0.84 eV in crystalline state[29].

Some other experimental results also support the double injection model. Nishimura *et al.*[30] measured the IR absorption of colored WO_3 films using D_2O and observed a strong absorption peak at approximate 1 μm, which could be ascribed to the absorption of W^{5+}, and another small but distinct absorption peak at 4.3 μm, which could be ascribed to the O–D

stretching vibration. These results revealed the role of proton injection from the electrolyte in the coloration process.

On the other hand, some other experimental results, for instance, coloration under UV illumination without H^+ (or cations) injection, can not be explained by the double injection model. Muramatsu *et al.*[31] compared the SIMS (Secondary Ion Mass Spectroscopy) spectra of electrochemically colored and bleached WO_3 films and found that there are no distinct differences in the kind of element and the spectral peak heights of H^+, also the OH and H_2O contents were the same in both cases. From these results, it was concluded that no hydrogen injection occurred during coloration. However, the results of Muramatsu *et al.*[31] supported Deneuville's tentative model. In 1980, Deneuville *et al.*[32] proposed that coloration results from the transfer of hydrogen from a passive to an active site within the WO_3 film, and that no H^+ was added. This transfer may be controlled by the electrochemical potential of hydrogen which may act as the driving force.

The results of electron spin resonance (ESR) studies also argue against both intervalence transfer and small polaron models[33]. Pifer *et al.*[33] suggested that if coloration is due to W^{5+}, the electrons are localized over large regions containing a number of W sites and not uniquely located in H_xWO_3.

Therefore, none of these models is fully valid and can explain completely the mechanism of electrochromism in WO_3 films. However, for comparison, the double injection model is considered to be the more reasonable explanation and is thus widely accepted.

1.3.2 Formation of Tungsten Bronze

Figure 1.4 shows the process of coloration and bleaching within WO_3 films according to the double injection model. During the coloration, electrons supplied by a negative polarity and protons supplied by ion storage, such as an electrolyte, inject into the WO_3 layer forming tungsten bronze H_xWO_3. During bleaching, electrons and protons are depleted from the H_xWO_3 layer by reversing the bias of electrodes[5].

H_xWO_3 belongs to a general class of nonstoichiometric mixed oxides of general formula $M_xA_yO_z$ ($0<x<1$), where M is a monovalent ion such as H^+, Li^+, Na^+, K^+, Ag^+ and Rb^+, and A_yO_z is a transition metal oxide.

The crystal structure of H_xWO_3 has been studied extensively[34–37]. Tungsten bronze exhibits a similar structure which progresses from distorted WO_3 to the cubic ReO_3 structure at high x values and varies with x[37]. Several crystal structural types of H_xWO_3 are known. It is tetragonal at x=0.1 with lattice parameters a=5.207Å c=3.869Å[34]; tetragonal at x=0.23 with a=5.228Å c=3.881Å[35]; tetragonal at x=0.33 with a=3.751Å c=3.796Å[36] and cubic at x=0.5 with a=3.755Å[36]. Wiseman *et al.*[37] studied the cubic structure of $D_{0.53}WO_3$ by neutron diffraction. They found by deuterium analogue that the tungsten atoms are arranged on a primitive cubic lattice and are surrounded by nearly regular octahedrons of oxygen atoms linked together by corner sharing. The octahedrons are tilted 11^0 from the –W–W– direction resulting in an O–O distance between adjacent octahedrons of

3.264Å. The deuterium atoms are statistically attached to all the oxygen atoms as deuteroxyl bonds O–D of 1.10Å length and 11.8^0 displacement off the line to the neighboring oxygen atom[37]. The structural investigations of the tetragonal hydrogen bronze phase shows marked similarity to the cubic hydrogen bronze structure[37].

Other tungsten bronzes, such as Li_xWO_3 and Na_xWO_3, have also been investigated[38-41]. Their properties and characteristics are similar to those of H_xWO_3. But it has been argued that the presence of Li^+ in Li_xWO_3 may result in a longer lifetime than H_xWO_3 since hydrogen tungsten bronze in the presence of O_2–saturated electrolyte H_2SO_4 is unstable while Li_xWO_3 is highly stable[38].

1.4 Optical Application of Electrochromic WO_3.

WO_3 material is used for display devices and in window applications with dynamic optical switching control due to their electrochromic properties. Basically, amorphous WO_3 film can be used in display devices because of its fast response of coloration and polycrystalline film can be used in window applications due to its high infrared reflectance during the coloration[1,2,12,22].

Kamimori *et al.*[4] reported electrochromic devices suitable as an antidazzling mirror for motor cars. The lifetime for repetitive operations is more than 10^5 cycles. Many investigators have been interested in window applications for the reason of obtaining solar energy efficiency[1,2,22,42,43].

Controlling radiant energy transfer through windows can lead to energy savings. If the onset of high reflectance occurs at a wavelength of $\lambda \approx 0.7$ μm, such windows can decrease the inflow of infrared solar radiation thereby diminish the need for air conditioning in a warm climate. If the onset of high reflectance is instead at $\lambda \approx 2.5$ μm, the windows can provide low thermal emittance and increase the energy transmittance in a cold climate. These desirable properties can be achieved by modulating the infrared reflectance. An idealized case is illustrated in Figure 1.5. A gradual increase in the reflectance energy is obtained as the reflectance edge moves towards shorter wavelengths. The electrochromic cell can modulate the reflectance properties. When the EC cell operates in the bleached state, it has high transmittance and low reflectance. At the colored state, the EC cell becomes deeply blue and has high reflectivity. Cogan *et al.*[10] measured the reflectance of a rf sputtering polycrystalline WO_3 films as a function of Li^+ injection and reported the reflectance of deeply colored WO_3 films exceeds 55% at a wavelength of 2.5 μm while the reflectance is about 15% for the bleached state. Some other authors have investigated the optical parameters of electrochromic WO_3. It was found that the refractive coefficient is about 2.2[6,8,9] and that the relative dielectric constant is about 4.8[1,42]. Schirmer *et al.*[15] measured the optical density of as-evaporated and colored WO_3 films. They observed that the optical density of colored film increases about 5–6 times depending on the injected electron density during coloration. The authors also reported that the absorption and reflectance spectra of crystallized layers are different from those of amorphous samples. Many authors[[10,12,15,41,44] have provided convincing evidences for the validity of the free-electron

Drude model to explain the reflectivity modulation observed in polycrystalline electrochromic WO_3. The optical absorption and reflectance are primarily determined by the density and scattering of the free electrons.

1.5 Subject of Research and Structure of Thesis

The aim of this thesis is to investigate quantitatively the variations in the electrical resistivity and carrier concentration of freshly prepared and intercalated WO_3 films; and to discuss structural changes of WO_3 films during the coloration and the bleaching processes; and to study the optical properties, such as reflectance, for window applications.

The second chapter describes the preparation of WO_3 films by spray pyrolysis, the experimental arrangements for coloring and bleaching the WO_3 films, and the measurement techniques: interference fringe step measurements for thickness determination, Hall measurements for electrical properties, X-ray diffraction (XRD) studies for crystal structure, IR spectroscopy and Spectrophotometer for optical measurements.

Chapter 3 presents experimental results and discussions, and compares infrared reflectance measurements with theoretical results calculated from the Drude model. Finally, a conclusion is presented in chapter 4.

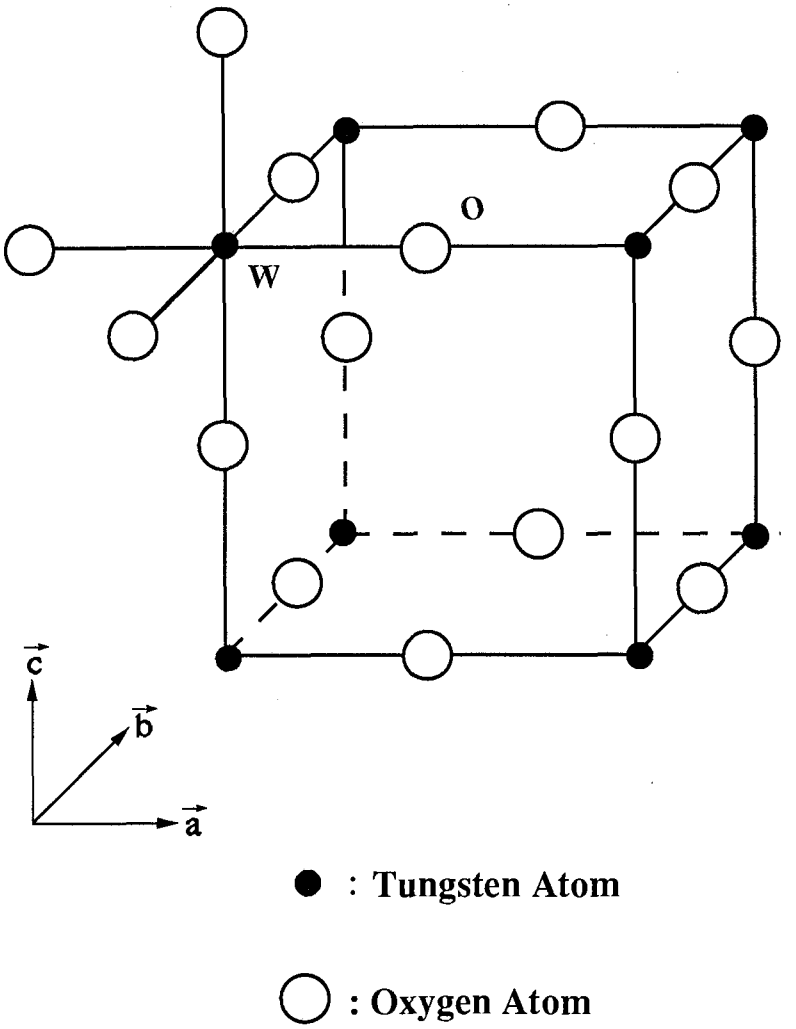

Figure1.1 WO_3 crystal structure with cubic approximation[23]

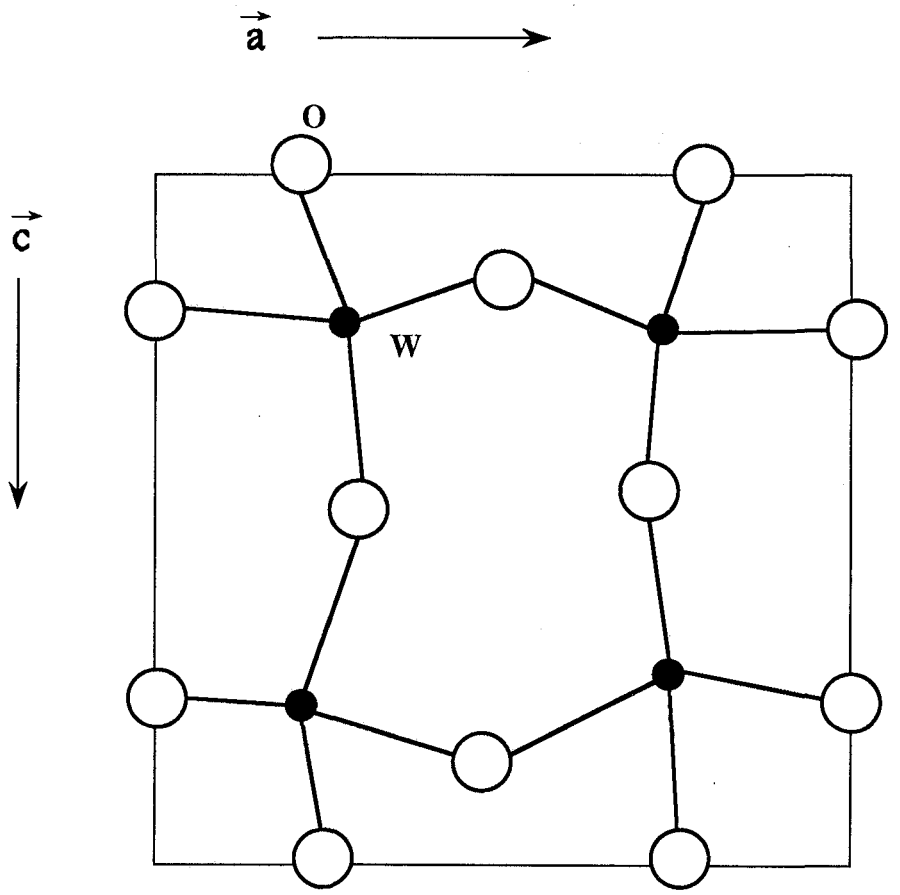

Figure 1.2 Projection in y axis of the distorted monoclinic WO_3 structure[23]

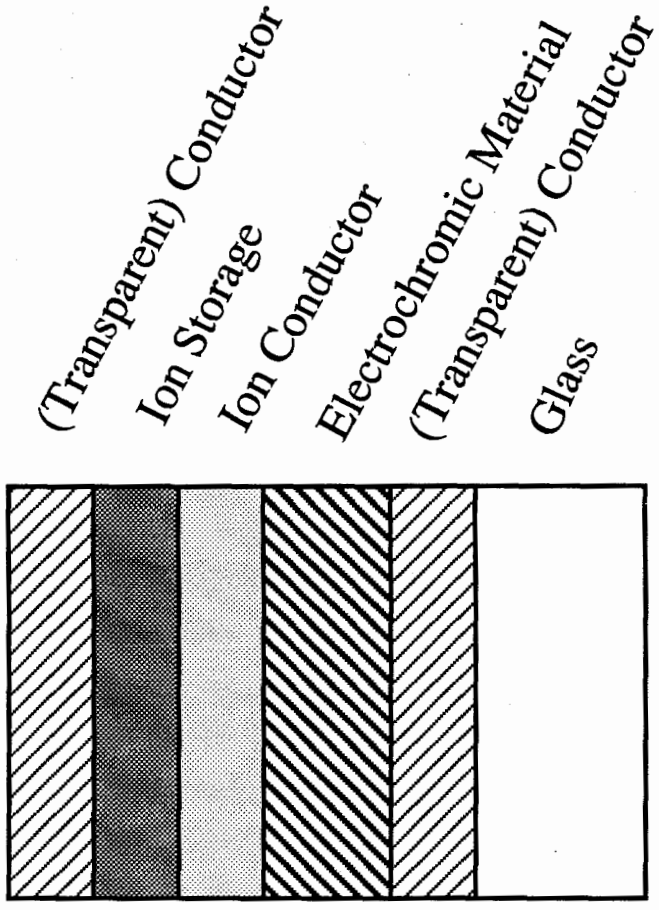

Figure 1.3 The sandwich structure of an electrochromic cell[1]

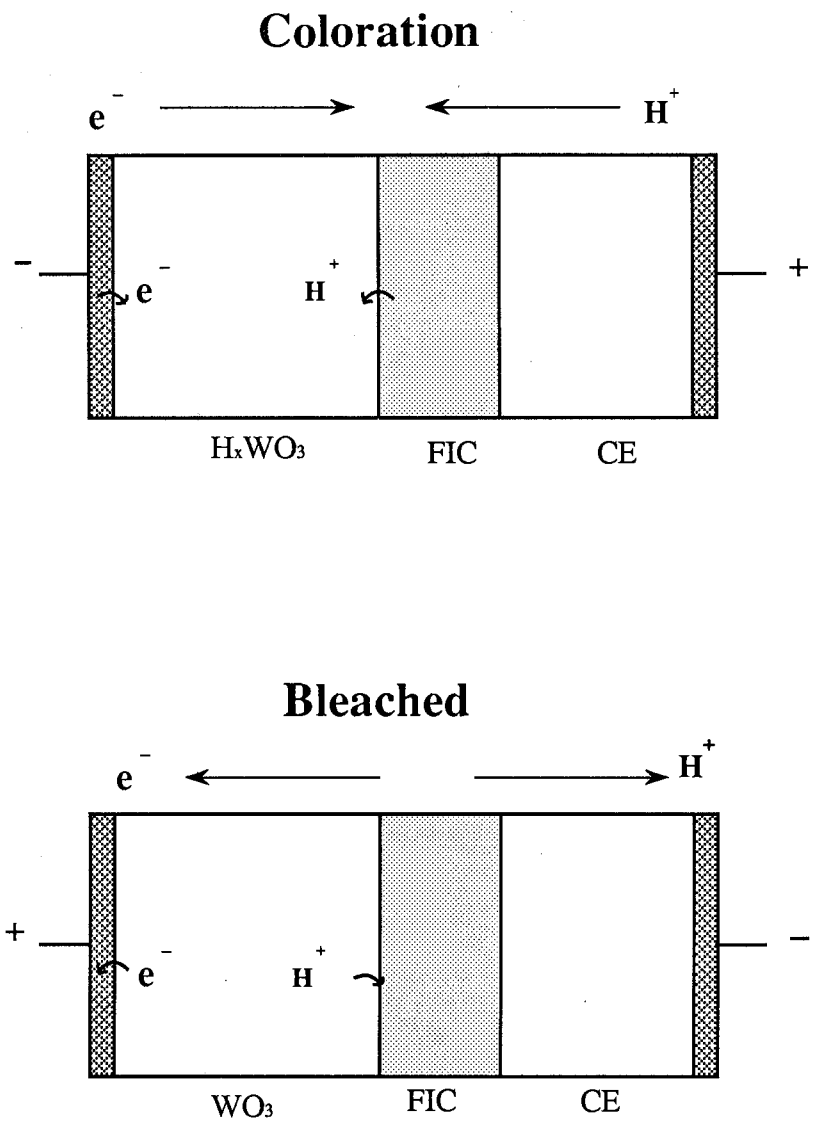

FIC: Fast Ion Conductor
CE: Counter Electrode

Figure 1.4 The process of coloration and bleaching reactions in an WO_3 film

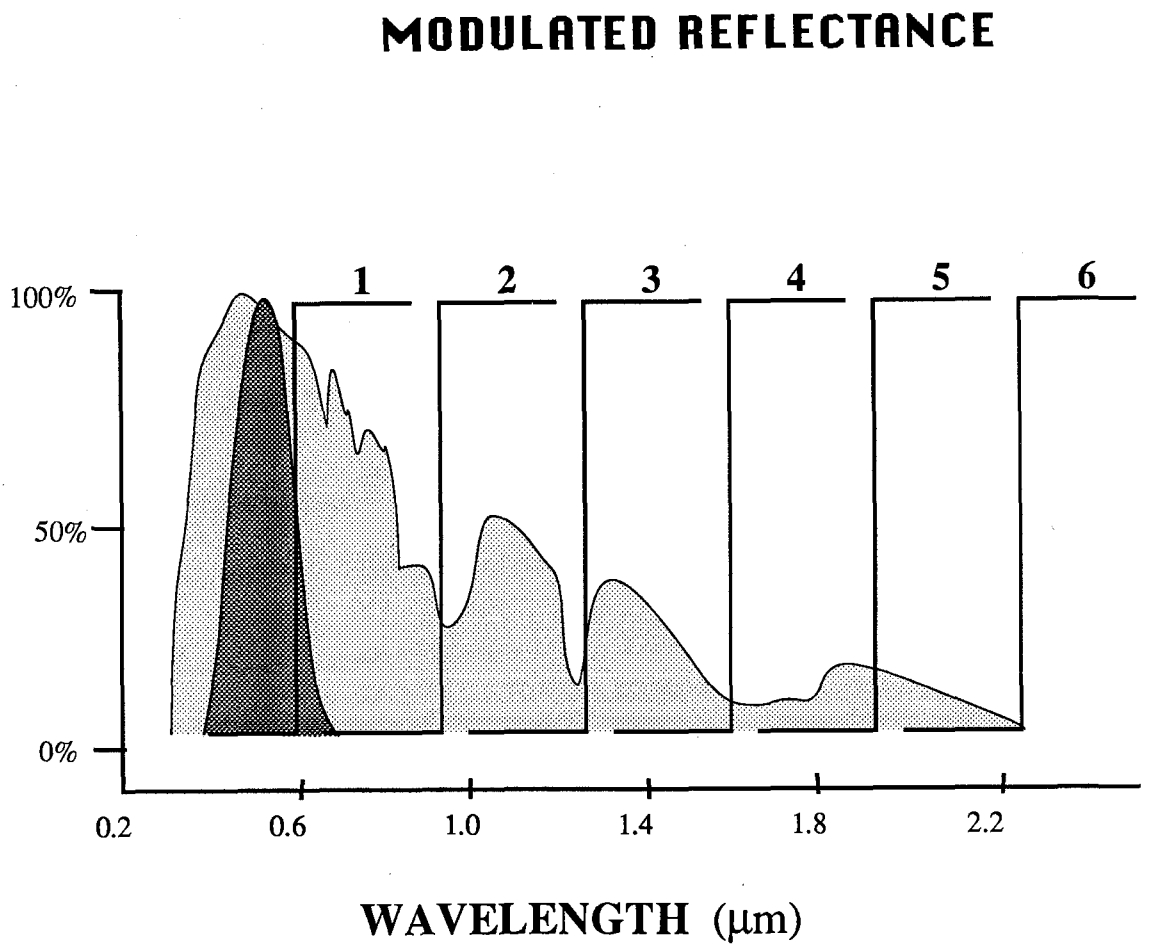

Figure 1.5 The infrared reflectance modulation for solar energy control[1]

Chapter 2

MATERIALS AND METHODS

2.1 Preparation of WO_3 Films

WO_3 films were prepared by spray pyrolysis. For each WO_3 film sample, 3.5 grams of tungsten chloride powder (Johnson Matthey Inc.) was dissolved in 100 ml N,N-Dimethyl Formamide (DMF) (BDA Chemicals Ltd.). The WCl_6 solution which is dark red in color was immediately sprayed.

Figure 2.1 shows the schematic set up for the preparation of pyrolytically spray deposited WO_3 films. An electronic nebulizer (EN145 Medigas Pacific Ltd. Burnaby, B. C.) was used to generate an aerosol of WCl_6. A powerstat variable transformer (3PN 116) was used to supply power for the electric heater and N_2 or air was used as a carrying gas. Prior to spraying, the substrate (Microscope slide or SnO_2:F glass (Ford)) was heated to the required temperature which was measured by a Chromel-Alumel Thermocouple attached to the substrate. During spraying, the heater with the substrate could move forwards and backwards to get a uniform film.

The chemical reaction of the pyrolytic process may be written as:

$$WCl_6 + \frac{3}{2}O_2 \longrightarrow WO_3 + 3Cl_2\uparrow \qquad (2.1)$$

The thickness of WO_3 films was controlled by varying the spraying time, and the substrate temperature was varied by changing the voltage of the transformer.

2.2 Experimental Arrangements for electrochemically coloring and bleaching WO_3 films

WO_3 films on glass were colored by attaching adhesive conducting copper strips to two opposite edges of films as shown in Figure 2.2. The electrolyte, poly (2-acrylamido-2-methyl-1-propane-sulfonic acid) (Aldrich Chemical Company Inc.), covered the entire surface of the films. A DC voltage of 1.5 V was applied across the sample, causing a blue color to originate at the cathode and then propagate towards the anode. This experimental arrangement can not be used for bleaching the films, since when reversing the polarity of the voltage, the bleaching appeared first at the anode; on continued application of the voltage, the coloration appeared again at the newly formed cathode. Figure 2.3 shows the experimental arrangement for obtaining both coloring and bleaching states. The samples were colored when a negative voltage of 1.5 V was applied to the WO_3 film, while the

bleaching state was achieved by reversing the bias of the WO_3 electrode. After coloration or bleaching, the WO_3 samples were washed with distilled water, and dried in an air stream.

For coloring and bleaching WO_3 films on SnO_2:F glass, the same experimental arrangement as shown in Figure 2.3 was used. However, since the SnO_2 film acted as the electrode, the entire WO_3 film was kept at a constant potential and a uniform coloring or bleaching was observed immediately. Thus, the experimental arrangment shown in Figure 2.3 with the use of the WO_3 film deposited onto the SnO_2:F substrate was used as an electrochromic cell (EC cell).

2.3 Measurement of Film Thickness

For the thickness measurement of SnO_2:F and WO_3 films, four random holes were made in each film by placing a small amount of Zn powder on the film and then adding a drop of concentrated HCl solution. After reaction, the mixture was rinsed from the film with distilled water and dried. The thickness of the film was then measured by interference fringe step method (Wild Microscope 20, Wild of Canada Limited). The measured error is estimated at ±20 nm.

2.4 Resistivity and Hall Coefficient Measurement

The resistivity and Hall coefficient of samples were measured by using Van der Pauw's technique[45,46] at room temperature. As shown in Figure 2.4, tungsten films on glass were cut into 25.45 ± 0.02 mm squares, and four-point contacts (**M, N, O, P**) with a separating space of 13.68 ±0.02 mm were mounted on a suitable holder. A current $\mathbf{i}_{mn}$ was applied to contacts **M** and **N**, and the potential difference $\mathbf{V}_{p-o}$ was measured. With defining $\mathbf{R}_{mn,op} = \frac{\mathbf{V}_{p-o}}{\mathbf{i}_{mn}}$, the Hall resistivity was obtained by the following formula[46]:

$$\rho = \mathbf{R}_{mn,op} \cdot \mathbf{d} \cdot \mathbf{C}_r \qquad (2.2)$$

where $$\mathbf{C}_r = \frac{2\pi}{\ln 2 + 2\ln[1+2(\mathbf{c/b})^2] - \ln[1+4(\mathbf{c/b})^4]}$$

and **d** is the thickness of the film; **c/b** is the ratio of the separating space between contacts **M** & **P** and the length of the square sample. For the Hall coefficient measurements, a uniform magnetic field **B** of 1 – 15 kG was applied perpendicular to the plane of the sample, the contacts **M** and **O** were used as current probes, and the contacts **N** and **P** as voltage probes.

The Hall coefficient is given by[46]:

$$\mathbf{R}_H = 10^8 \frac{\mathbf{d}}{\mathbf{B}} \cdot \frac{(\mathbf{V}-\mathbf{V}_0)}{\mathbf{i}_{MO}} \mathbf{C}_H \qquad (2.3);$$

where $C_H = \left(\frac{1}{2} + \frac{\tan^{-1} 2(c/b)^2}{\pi/2} \right)^{-1}$

is a correction factor for the Hall coefficient; **V** and V_0 are the potential difference between points **N** and **P** in volts with the magnetic field **B** applied and with no applied field respectively; **d** is the film thickness in cm and i_{MO} the current between points **M** and **O** in amperes.

Then, the carrier concentration is obtained by the relation[45]:

$$n_e = \frac{1}{R_H e} \qquad (2.4)$$

where e is the charge of electron.

For all samples, the size effect may be ignored because the thickness of films was larger than 200 nm[47]. In the Hall coefficient measurements, the Hall voltage change ($V-V_0$) was found to vary linearly with the applied magnetic field as shown in Figure 2.5. For all measurements, an average value of **V/ i** was obtained by taking five data points of the current **i** as a function of the potential difference **V.** The relationship between **i** and **V** was also linear as shown in Figure 2.6. The random error from the measurements was estimated to be about 5%.

2.5 X-ray Diffraction Studies

X-ray diffraction (XRD) spectra were obtained using an X-ray generator

system (Model: PW1730 Philips Electronic Instruments Inc. Mahwah, N. J.) with CuKα radiation. The voltage applied to the X-ray tube was 50 kV and the current was 35 mA. By analyzing peaks in the diffraction pattern of the polycrystalline samples, the space between adjacent parallel lattice planes (d-spacing) was found from the Bragg relation[48]:

$$\mathbf{d} = \frac{\lambda}{2\sin\theta} \qquad (2.5)$$

where λ is the wavelength of CuKα radiation, and θ is the diffraction angle. The diffraction peaks were assigned to the corresponding crystal planes by comparing the experimental d-spacing from the diffraction pattern and theoretical d-spacing calculated from the lattice parameters and Miller indices (hlk) given in [48].

For monoclinic WO_3 film, the theoretical d-spacing was obtained by using the following formula[48]:

$$\frac{1}{d^2} = \frac{\frac{h^2}{a^2} + \frac{l^2}{c^2} - \frac{2hl\cos\beta}{ac}}{\sin^2\beta} + \frac{k^2}{b^2} \qquad (2.6)$$

where the lattice parameters are a = 7.302Å, b = 7.530Å, c = 3.846Å and $\beta = 90.88^0$[19].

For tetragonal SnO_2 film, the d-spacing was calculated from the following formula[48]:

$$\frac{1}{d^2} = \frac{h^2}{a^2} + \frac{k^2}{b^2} + \frac{l^2}{c^2} \qquad (2.7)$$

where a = b = 4.747Å, and c = 3.191Å[49].

2.6 Optical Measurements

The infrared reflectance spectra of SnO_2 films, as-prepared and colored WO_3 films on glass and SnO_2 coated glass were measured using Infrared Spectroscopy (Model: Bruker IFS 113V); and the reflectance and transmittance spectra for the visible region of the light spectrum were obtained by a spectrophotometer (Model: CARY 17).

Figure 2.7 shows the experimental set up for the time response measurement of the EC cell. It consists of an x-y recorder (7000AR, Hewlett Packard), a monochromator (Spex, Industries Co., Metuchen, N. J.) and a Schottky barrier silicon pin photodiode (PIN-6LC, United Detector Technology Inc., Santa Monica, Cal.) which has a linear response to visible and near-infrared lights. The incident light source was a tungsten halogen lamp which has a steady output intensity.

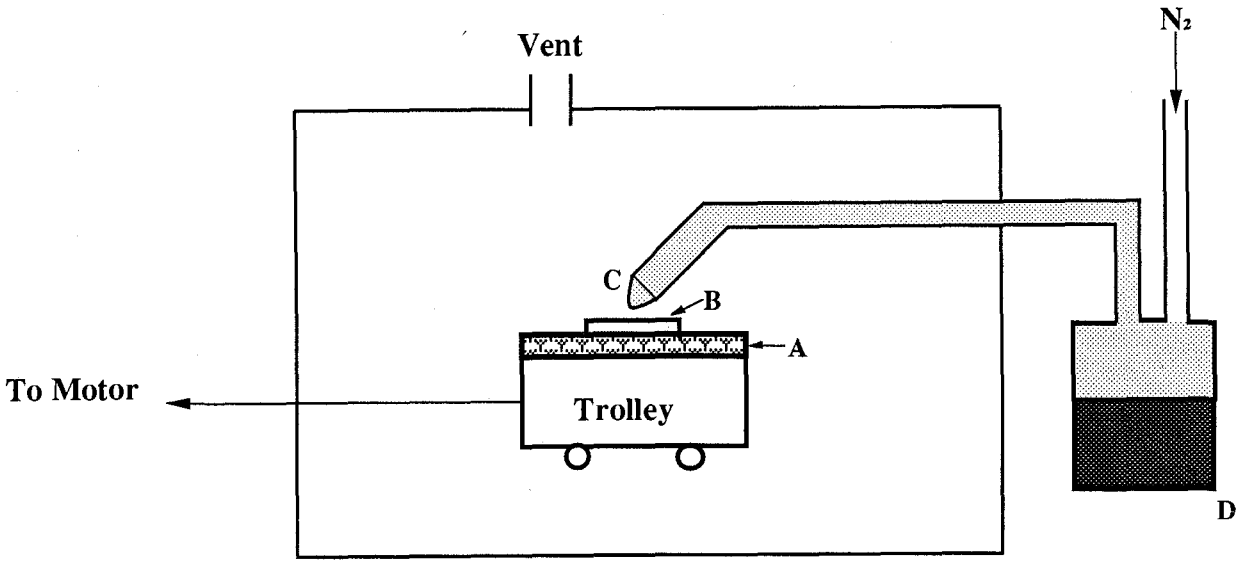

A: Electrical Heater
B: Substrate
C: Spray Nozzle
D: Nebulizer

Figure 2.1 The schematic of pyrolytic spray deposition unit

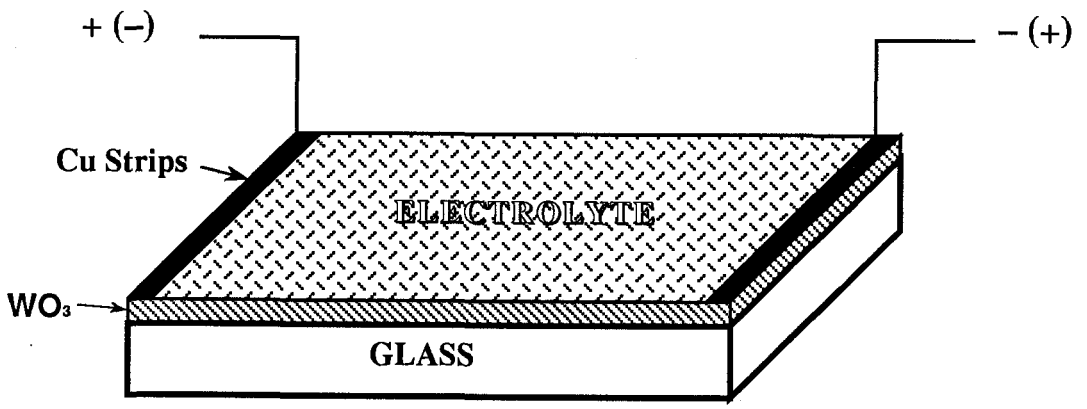

Figure 2.2 Experimental arrangment for coloring WO_3 films deposited onto glass slide

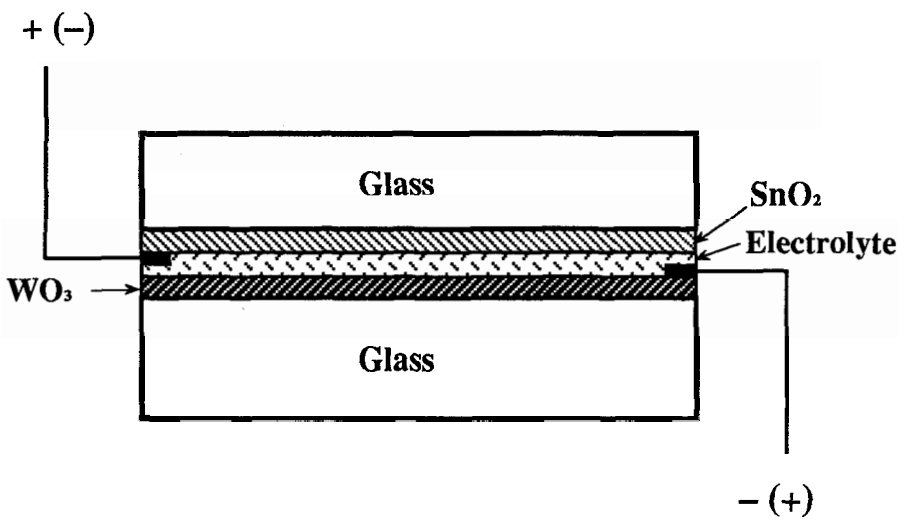

Figure 2.3 Experimental arrangment for coloring and bleaching WO_3 films deposited onto both glass and SnO_2:F substrates

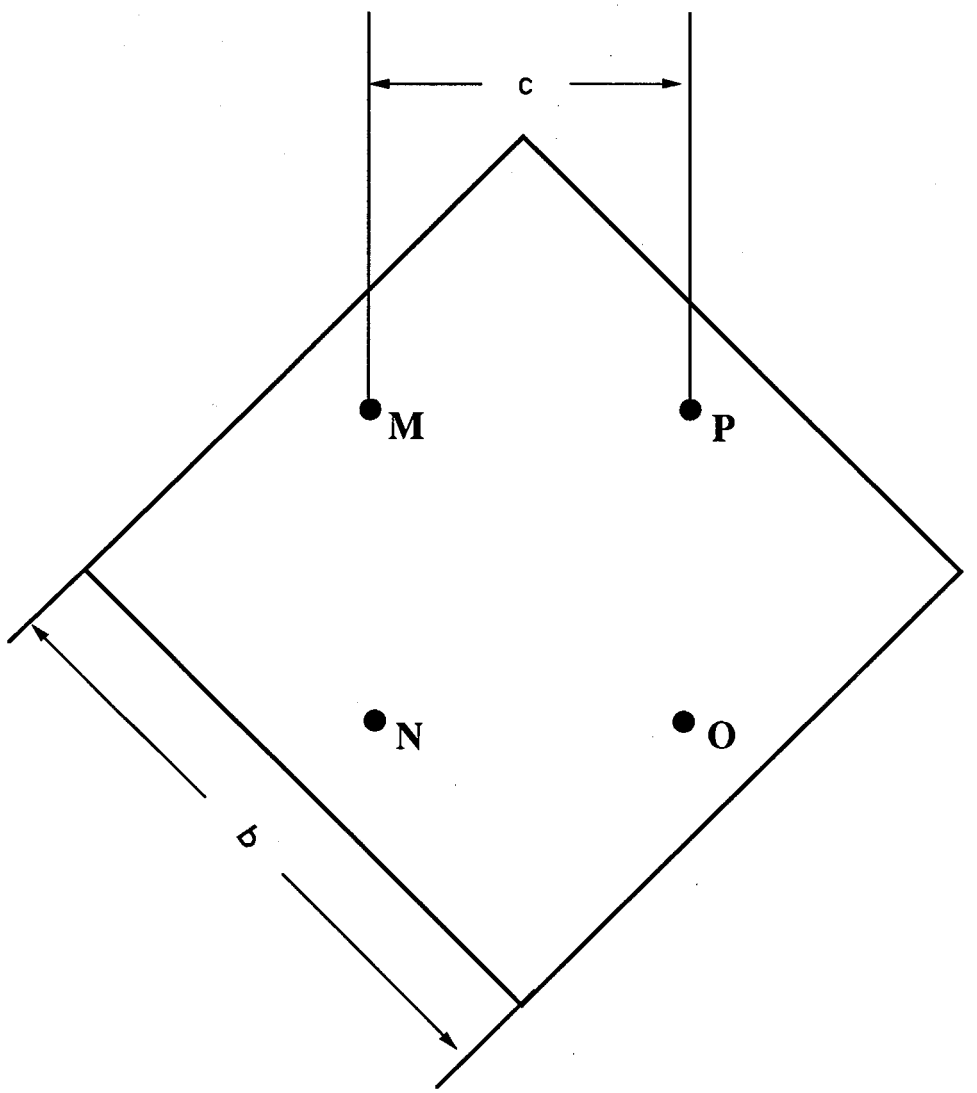

Figure 2.4 The diagram for Hall measurements showing a separating spacing of four-point contacts c=13.68 mm, and the length of squares sample b=25.45 mm

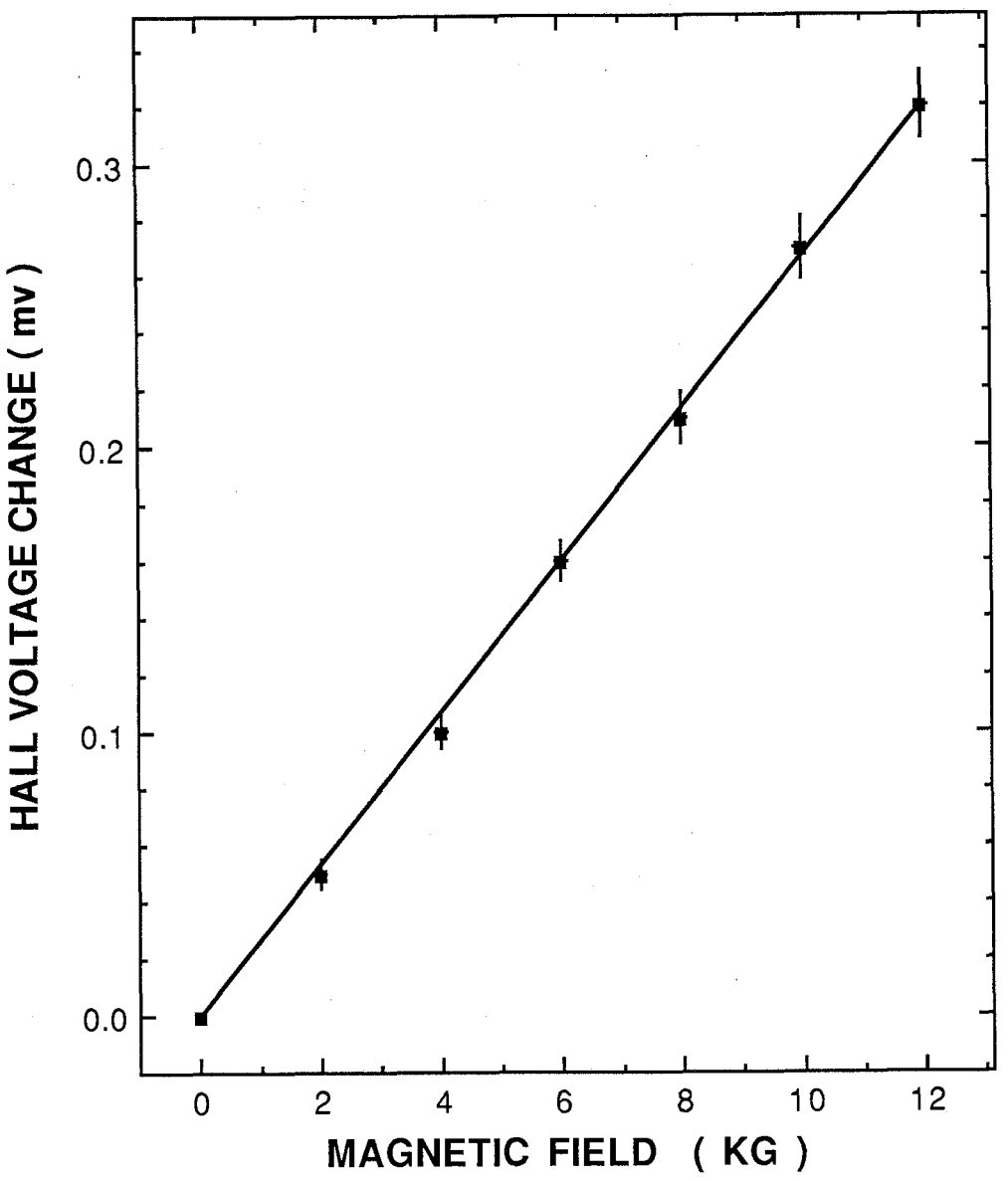

Figure 2.5 The relationship between the Hall voltage change ($V-V_0$) and the applied magnetic field B with the current I_{Mo} constant for WO_3 film prepared on glass at 350°C

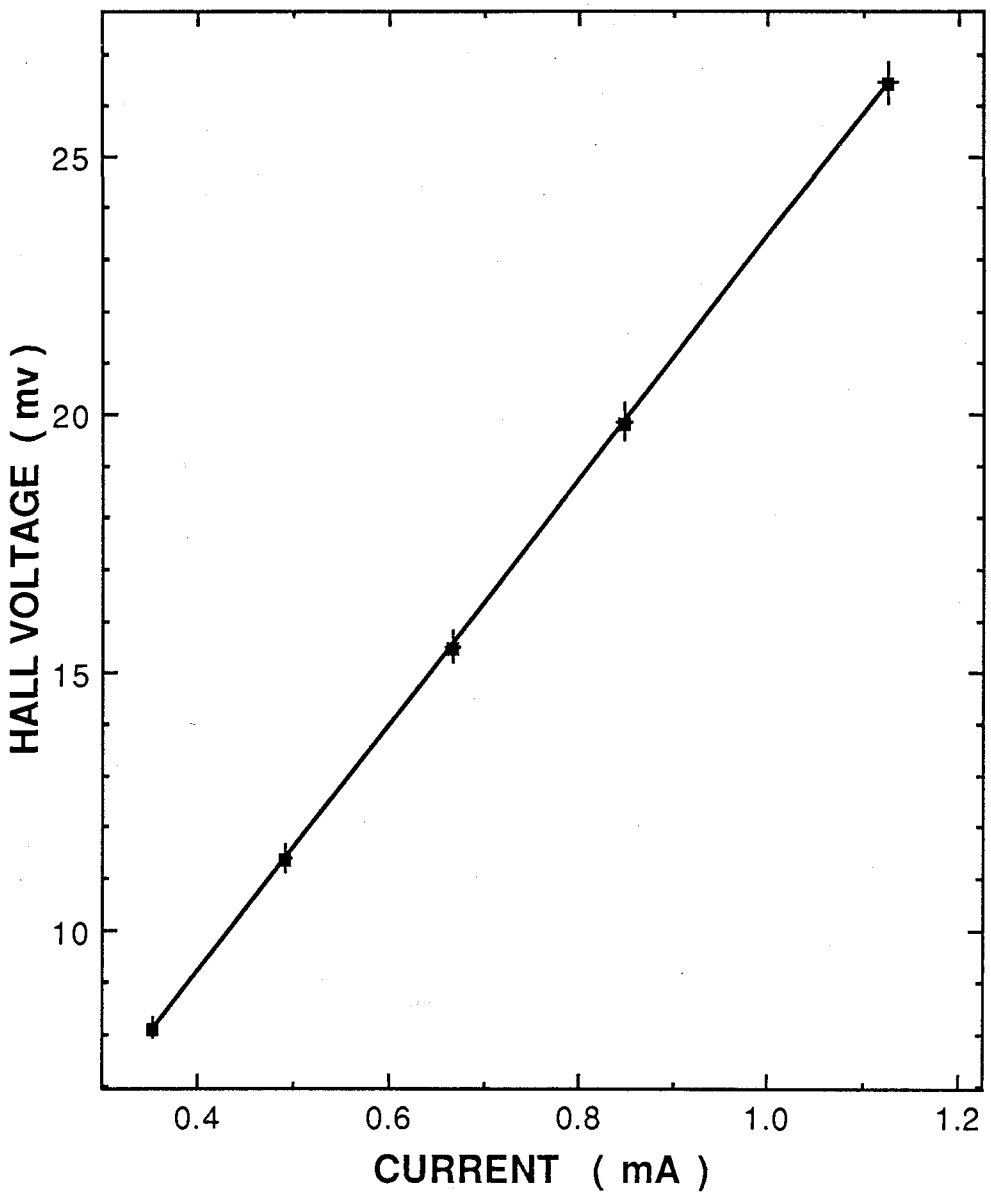

Figure 2.6 The relationship between the applied current I_{Mo} and the Hall voltage V while keeping B constant for WO_3 film prepared on glass at substrate temperature 350°C

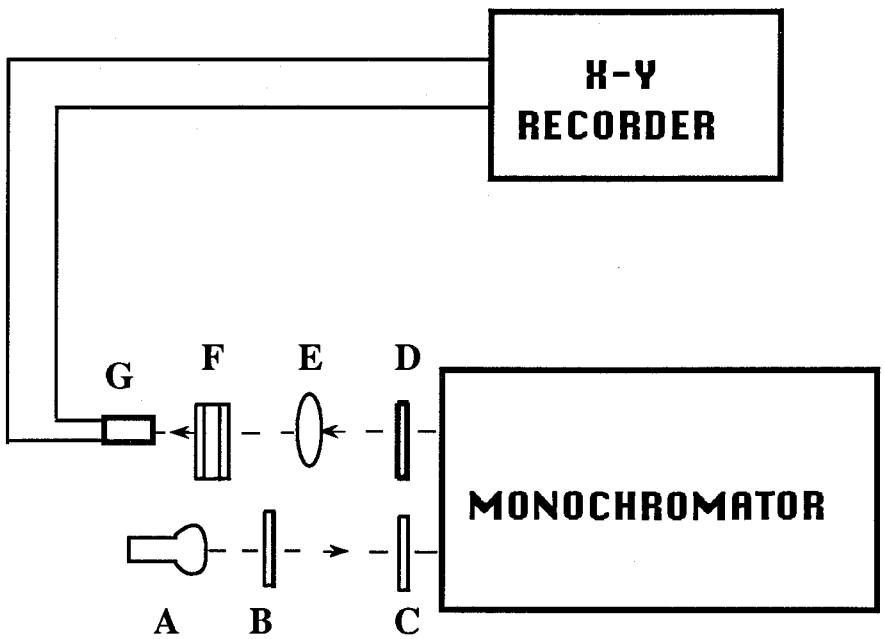

A: Tungsten Halogen Lamp
B: Filter
C: Chopper
D: Slit
E: Lens
F: Electrochromic Cell
G: Photodiode

Figure 2.7 The experimental set up for electrochromic measurement

Chapter 3

RESULTS AND DISCUSSIONS

3.1 Properties of WO_3 Films

3.1.1 Crystallinity of WO_3 Films

The crystallinity of pyrolytic spray deposited tungsten trioxide films is strongly dependent on the deposition temperature. Figure 3.1 shows the typical X-ray diffraction patterns for WO_3 films deposited on a glass slide at substrate temperatures of 250°C, 300°C, 350°C and 400°C. The thickness of the samples ranged from 400 nm to 500 nm. It was found that the films prepared at temperature above 300°C were polycrystalline in nature while those at below 300°C were amorphous. By comparing the d-spacing calculated from the lattice constants of monoclinic WO_3[19], the main peaks in the X-ray diffraction patterns of polycrystalline films were assigned to the planes WO_3(001), (020), (200), (210), (021), (201), (002), (112), and (022). The films were predominantly oriented with the (001) plane parallel to the substrate surface. The observed diffraction patterns were similar to those obtained by Miyake *et al.* on vacuum evaporated films[6]. In addition, additional weak peaks were observed in the diffraction patterns of some

films and could be attributed to sub-oxides WO_{3-x} ($0<x<3$) as the minor phase[6]. However, the pyrolytically spray deposited WO_3 films had a main composition of tungsten trioxide. This was also confirmed by XPS measured by Craigen *et al.*[14].

Generally, a transparent conducting SnO_2:F film was used as both, the substrate film for electrochromic layer and the counter electrode in EC cell to achieve a fast response during coloration and bleaching. SnO_2:F films on glass (Ford glass) have a low sheet resistivity of 35 $\Omega/\square$, and a thickness of 220±20 nm. X-ray diffraction studies revealed that the films are polycrystalline in nature and their diffraction peaks were mainly due to SnO_2 planes (110), (200), (211) and (310). Figure 3.2 shows X-ray diffraction patterns for a WO_3 film on the glass substrate, the SnO_2:F film and a WO_3 film on the SnO_2:F film substrate. Both the WO_3 films on glass and on SnO_2:F were deposited at 350°C, and had thickness of 400±20 nm. The observed diffraction patterns of the WO_3 films on SnO_2:F are mixtures of structures of WO_3 and SnO_2. Also, additional X-ray diffraction peaks were observed in the diffraction pattern of WO_3 film on the SnO_2:F substrate than in WO_3 film on the glass substrate at the same deposition temperature. This may be due to the different substrate surfaces being used and that WO_3 films will grow more easily on a polycrystalline substrate. A higher crystallinity of the substrate will yield a better crystallinity of WO_3 film[50]. Therefore, the nature and smoothness of the substrate surface can influence the atomic mobility and diffusion of the surface atoms during the deposition and hence the crystalline structure of the film during deposition[51].

Figure 3.3 shows the X-ray diffraction patterns of WO_3 films deposited onto SnO_2:F at substrate temperatures of 250°C, 300°C and 400°C. At 250°C, no diffraction peak could be attributed to WO_3. However, samples deposited above 300°C have several diffraction peaks which could be assigned to WO_3 planes. Many more peaks were observed when the films were deposited at the higher temperature of 400°C. Figure 3.3 reveals that the WO_3 films deposited onto SnO_2:F at temperatures below 300°C are amorphous and above 300°C are polycrystalline in nature. This is consistent with the results of WO_3 films deposited on glass slides as discussed above.

3.1.2 Resistivity of WO_3 Films

The thickness of pyrolytically spray deposited WO_3 films ranging from 250 nm to 650 nm were obtained by varying the deposition time from 10 minutes to 25 minutes while all other deposition parameters, such as flow rate, remained constant. Zhou[52] found that the thickness of films is proportional to the flow rate and that films deposited at high temperatures (>300°C)with a flow rate of 16.5 L/min. have a more randomly oriented crystalline structure and larger crystalline size. For our samples preparation, the flow rate of 17 L/min. was used.

Figure 3.4 shows the dependence of the resistivity of pyrolytically spray deposited WO_3 films on the deposition temperature. It was found that the resistivities of WO_3 films varied from 10^5 to 1 Ω·cm for the temperature

range from 200°C to 400°C, respectively. The thickness of the films ranged from 400 nm to 500 nm.

As shown in Figure 3.4, the resistivity decrease with increasing deposition temperature (> 200°C) is in agreement with results by Miyake *et al.*[6] on vacuum evaporated WO_3 films. The authors also reported that the resistivity of films deposited at temperatures between 50 and 200°C is essentially independent of the deposition temperature.

The relationship between the resistivity and thickness of WO_3 films was also investigated. The resistivities of films with a thickness ranging from 300 nm to 600 nm and deposited at 350°C were on the order of 10 Ω·cm and essentially independent of film thickness. However, Miyake *et al.*[6] observed the increase in the resistivity with decreasing film thickness for thinner films (< 200 nm).

The resistivity of WO_3 films deposited onto SnO_2:F were not determined, since the SnO_2:F film has a much lower resistivity than WO_3 films thus influences the determination of resistivity of WO_3 films.

The density of tungsten oxide films prepared at 350°C was estimated to be 6.5±0.3 g/cm^3 by using the measured values of the thickness, area and weight of the oxide films. The result is consistent with films prepared by other deposition techniques[6,8,9]. The density of WO_3 films is substantially smaller than that of a single crystal bulk sample of WO_3 (7.3 g/cm^3)[8]. This is likely due to a large number of defects and grain boundaries in the WO_3 films. During the preparation process, many structural defects, such as oxygen ion vacancies, are introduced in oxide films. The films have

substantial porosity which is assigned to the presence of these defects[6]. However, the high porosity or low density in WO_3 films is an advantage for electrochromic property because electrons and protons can easily diffuse into films.

3.2 Comparisons of Uncolored, Colored and Bleached WO_3 Films

3.2.1 Electrical Properties of Electrochromic WO_3 Films

3.2.1.a) Coloration Phenomena

Tungsten trioxide films were colored by applying a small DC voltage across the films with the use of electrolyte as described in 2.2. The liquid electrolyte Poly-Amps which covered the surface of the films is a transparent polymer and is well suited for WO_3 display applications[5,53,54]. A small DC voltage (usually $0.5\ V < v < 2\ V$) was applied across the electrodes in order to supply a driving force to transfer electrons and protons into WO_3 films. The coloration of WO_3 films on the glass slide substrate was completed within minutes, while Deb[5] applied a large electrical field of 10^4 V/cm to color evaporated WO_3 film in the absence of an electrolyte and found that the coloration process required several hours at room temperature depending on the presence of moisture. The increase in the rate of coloration in the presence of the electrolyte in our

experiment likely arises from protons of the electrolyte be injected into the WO_3 film. In Deb's experiment, the coloration depended on the presence of moisture to obtain proton injection. It was found that no coloration effects were observed for samples maintained under high vacuum or at temperatures above 350°C[27]. This was attributed to loss of H_2O from the films. Thus hydrogen ions (or water) play a dominant role in the coloration phenomena.

It was also observed that the coloration process was completed immediately for WO_3 film on SnO_2:F substrate, while for WO_3 on the glass substrate the coloration originated at the cathode then propagated toward the anode and completed in few minutes. Increase of response time for WO_3 films on SnO_2:F is likely due to the highly conducting SnO_2 layer as the substrate of the WO_3 film, which acts as the electrode. The time for coloring the entire area (25.45 mm squares) of WO_3 film on the glass substrate under a constant applied voltage (1.5 V) was dependent on the thickness and deposition temperature of the film. The results are listed in Table 3.1 and will be discussed later.

3.2.1 b) Variation of Electrical Properties

Figure 3.5 shows the dependence of the electrical resistivity of uncolored and colored film on the deposition temperature. The curve (A) in Figure 3.5 is the resistivity of fresh-prepared WO_3 films as presented in Figure 3.4, and the curve (B) is the electrical resistivity of same WO_3 films after

coloration for about 3 minutes. It is found that the electrical resistivities decrease by 2 to 8 orders of magnitude after coloration. The resistivities of colored WO_3 films were on the order of 10^{-2} Ω·cm and seems to be independent of the deposition temperature or the structure of oxide films. The carrier concentration of all colored films was estimated by Hall measurements to be in the range of 10^{20} to 10^{21} cm^{-3}. The injection of the large number of carriers during coloration is attributed to the special structure of WO_3. It was found that WO_3 has an "extended defect" structure, in which voids or vacancies can be continuously filled by the ions M up to x=1 forming tungsten bronze M_xWO_3[28], i.e. the injected ions concentration can equal to the number of W atoms. The physical properties of M_xWO_3 vary with x and it was found to be metallic for large values of x[5,55]. According to the double injection model, electrons and protons take part in the electrochromic process. The electrons supplied by the negative polarity of the voltage source propagate into the WO_3 films, and the electrolyte, which covers the surface of the WO_3 film, supplies protons to neutralize the electron space charge in the WO_3 film. In the electrochromic process, the diffusion speeds of electron and proton D_e and D_p respectively are very different. It was found that the proton diffusion coefficients D_p are $1.8 \cdot 10^{-10}$ and $1.4 \cdot 10^{-11}$ cm^2/sec for amorphous and crystalline samples respectively[56]; while D_e is about 0.0025 cm^2/sec for electrons in the amorphous films and 0.25 cm^2/sec in single crystal[25]. The protons which diffuse much more slowly than electrons in WO_3 do not limit the electrochromic process, since the protons from the electrolyte need only to diffuse a small distance into the WO_3 layer (~ 400 nm), while the electrons have to move several millimeters from the point of contact for WO_3 on glass.

Figure 3.6 shows the dependence of the resistivity and carrier concentration on film thickness of colored WO_3 films deposited at 350°C. The uncolored films have resistivities on the order of 10 Ω·cm. After coloration, the resistivities decrease to 10^{-2} Ω·cm, and are essentially independent of film thickness. However, the resistivity of the 600 nm thick sample is somewhat higher due to the fact that the resistivity and the carrier concentration were measured after a constant coloration interval (3 minutes) for all samples of various thickness. Since thicker samples possess a larger volume space, a longer intercalation time would be required to reach the same resistivity and carrier concentration as thinner films. This effect is also observed in Table 3.1. The intercalation time required to color the entire area was doubled when the sample's thickness increased from 450 nm to 600 nm.

The time dependence of the resistivity and concentration of WO_3 films was also investigated and the results are shown in Figure 3.7. When the voltage was applied across the polycrystalline sample prepared at 350°C with a thickness of 400 nm, the carrier concentration increased rapidly within 1 to 2 minutes and reached a plateau after about 6 minutes. This illustrates that the intercalated electrons are limited by a certain value of x, which allows the structure to accommodate a certain number of electrons and protons. It is also observed that an amorphous film prepared at 250°C seems to have a higher plateau and reached the plateau more slowly. This is likely due to the structural disparity between the polycrystalline and amorphous samples. In the crystal structure, there are some channels allowing the electrons to diffuse easily into the WO_3 film, such as, in (001)

direction, the connection of oxygen octahedrons producing a hollow channel as shown in Figure 3.8. The radius of such channel is about 1Å[57]. Thus electrons can easily diffuse into these channels in crystalline samples. In addition, the polycrystalline WO_3 films have a smaller density of grain boundaries than amorphous films[50] and thus less electron scattering. The electrons injected into highly polycrystalline films show more likely free electron behavior, which results in faster diffusion of electrons. For the amorphous sample, electrons are diffusing more slowly due to the disordered structure. However, an amorphous sample is highly porous and has a large number of grain boundaries. The injected electrons will be preferentially trapped at deeper sites[15]. Therefore it is expected that more electrons can be injected into amorphous films than in polycrystalline films, i.e. an amorphous WO_3 structure can accommodate a larger number of electrons.

3.2.2 Structural Properties of Electrochromic WO_3 Films

3.2.2 a) Tungsten Trioxide Films on Glass Substrate

Figure 3.9 shows the X-ray diffraction patterns of the uncolored and colored WO_3 films prepared on glass slide at temperature 250°C. The XRD pattern of the colored film revealed that no distinct diffraction peak was observed after the film was colored. The result shows no change in the amorphous films during the electrochromic process.

The situation is different for polycrystalline films as shown in Figure 10 (a) and (b). On comparing the patterns of the original (uncolored) and colored films, it is found that their diffraction patterns are considerably different. Some diffraction peaks were not observed and new peaks appeared after the WO_3 films were colored. The X-ray diffraction peaks for colored WO_3 films can no longer be assigned to monoclinic WO_3. In fact, the experimental results reveal that structural changes take place during the coloring of the polycrystalline WO_3 films.

According to the double injection model, the coloration of WO_3 films is due to the formation of hydrogen tungsten bronze (H_xWO_3) by injection of electrons and protons into the films. The hydrogen tungsten bronze H_xWO_3 crystal structures vary with x, and the following types are reported: tetragonal $H_{0.1}WO_3$[34]; tetragonal $H_{0.23}WO_3$[35]; tetragonal $H_{0.33}WO_3$[36] and cubic $H_{0.5}WO_3$[36]. By comparing the experimental d-spacing with the theoretical d-spacing calculated from the lattice parameters and Miller indices (hkl), the diffraction peaks of the colored films can be assigned to planes of the tetragonal hydrogen tungsten bronze $H_{0.23}WO_3$.

Figure 3.10 (a) shows the X-ray diffraction pattern of original uncolored, colored and bleached films prepared at 350°C. The peaks at $2\theta = 23.60^0$ and 24.30^0 corresponding to planes WO_3(020) and (200) disappeared, and two new peaks were observed after the sample was colored. The two new peaks at $2\theta = 33.40^0$ and 47.95^0 may be assigned to planes (111) and (220) of hydrogen tungsten bronze ($H_{0.23}WO_3$) respectively. However, when the sample was bleached, the X-ray diffraction pattern changed to the original uncolored state. The comparison of the relative intensities of diffraction peaks for

uncolored, colored and bleached films is shown in Table 2.2. It seems that the X-ray diffraction peaks of the bleached film are the same as for the original uncolored film, but their relative intensities fluctuated about 10%.

Figure 3.10 (b) shows the similar results of the structural changes for a WO_3 film prepared at 400°C. After the sample was colored, the peaks at $2\theta = 23.60^0$, 24.30^0 and 33.65^0 corresponding to WO_3(020), (200) and (201) disappeared, and one new peak at $2\theta = 47.95^0$ corresponding to $H_{0.23}WO_3$ (220) was observed. Another peak at $2\theta = 33.30^0$ increased about 3 times in relative intensity and changed its structure from WO_3(021) to $H_{0.23}WO_3$(111). For all other peaks, a little shift in the peak position was observed. These peaks were assigned to the planes of the hydrogen tungsten bronze $H_{0.23}WO_3$. Table 3.3 lists the X-ray diffraction peaks, the d-spacing and the crystal planes of uncolored (WO_3) and colored ($H_{0.23}WO_3$) film prepared at 400°C. After the sample was bleached, the crystal structure returned to the original uncolored state similar to the sample prepared at 350°C. The comparison of the relative intensities of uncolored, colored and bleached films is also shown in Table 3.2.

In order to understand more clearly the structural changes during coloration, an intermediate process with a light blue color was observed. We can see from the curves **D** in the Figure 3.10 (b) that the relative intensities of peaks at $2\theta = 23.60^0$, 24.30^0 and 33.65^0 corresponding to WO_3(020), (200) and (201) respectively, reduced gradually and will disappear finally, however the peaks at $2\theta = 33.40^0$ and 47.95^0 corresponding to $H_{0.23}WO_3$(111) and (220), respectively increased substantially.

3.2.2 b) Tungsten Trioxide Films on SnO_2:F Substrates

The tungsten trioxide films on SnO_2:F substrates were also investigated. Figure 3.11 reveals the structural changes in the polycrystalline WO_3 films prepared on SnO_2:F substrate at 400°C. The X-ray diffraction patterns for this case are complex, because they involved the structures of WO_3 and SnO_2. However, it is reasonable to expect that the X-ray diffraction peaks of SnO_2 don't change during the electrochromic process. For the original uncolored WO_3 film, the main peaks of the X-ray diffraction patterns were assigned to the planes WO_3(001), (020), (200), (111), (201), (121), (221), (002), (012), (112), (022), (202), (122) and (212). After the sample was colored, some diffraction planes, such as WO_3(020), (200), (201), (121) and (012), disappeared, and the peaks in the diffraction pattern of the colored film may be assigned to the hydrogen tungsten bronze $H_{0.23}WO_3$. The XRD peaks, the d-spacing and the crystal planes of uncolored and colored films on SnO_2:F substrate are shown in Table 3.4. After the sample was bleached, the X-ray diffraction pattern returned to the original pattern of the colorless sample. Therefore, the observation of structural changes of WO_3 films on SnO_2:F during coloring and bleaching is similar to the WO_3 films on glass slides.

So far, the X-ray diffraction investigations reveal the structural changes during the electrochromic process in various polycrystalline WO_3 samples. The structural changes from the tungsten oxide to tungsten bronze during coloration is believed to be a result of the double injection of electrons from

the cathode and protons from the electrolyte, causing the formation of the hydrogen tungsten bronze structure. During bleaching, tungsten bronze is reversed back to the tungsten trioxide. The same structural changes during the coloring and bleaching were observed for 3–4 cycles in our experiments. It is reported that the lifetime for repetative operations is more than 10^5 cycles for electrochromic devices[4]. It is expected that the structural changes could be same for each cycle.

3.2.3 The Optical Properties of Electrochromic WO_3 Films

3.2.3 a) Visible and Near Infrared Reflectance

(1). Theoretical Model -- Drude Model

The electron and proton insertions into WO_3 films during coloration increase the electrical conductivity of the films which exhibit a metallic-like behavior. Many investigators have provided direct evidences for the validity of the free electron Drude model for polycrystalline electrochromic WO_3 films[10,12,15,41,44,58,59]. Therefore, the reflective optical properties of polycrystalline WO_3 films can be discussed theoretically in terms of the Drude model.

According to the Drude model, the complex dielectric function ε can be written as[1,60]:

$$\varepsilon = \varepsilon_1 + i\varepsilon_2 = \varepsilon_\infty + \frac{i}{\rho\varepsilon_0\omega} \qquad (3.1)$$

where ε_1 is the real part of the complex dielectric function while ε_2 is the imaginary part; ε_∞ is the high frequency relative dielectric function; ε_0 is the permittivity of free space; ω is the photon angular frequency; and ρ is the complex dynamical resistivity which is given by[61, 62]:

$$\rho = \frac{1}{\varepsilon_0\omega_p^2\tau} - i\frac{\omega}{\varepsilon_0\omega_p^2} \qquad (3.2)$$

$$\text{where} \quad \omega_p^2 = \frac{n_e e^2}{\varepsilon_0 m^*} \quad , \quad \tau = \frac{\mu m^*}{e}$$

where ω_p is the plasma frequency; τ is the mean time between collisions; n_e is the electron density; e is the charge of the electron; m^* is the effective mass of the electron; and μ is the mobility of electron.

Substituting equation (3.2) into the equation (3.1) results:

$$\varepsilon = \varepsilon_\infty - \frac{\omega_p^2\tau^2}{1+\omega^2\tau^2} + i\frac{\omega_p^2\tau}{\omega(1+\omega^2\tau^2)} \qquad (3.3)$$

$$\text{thus,} \quad \varepsilon_1 = \varepsilon_\infty - \frac{\omega_p^2\tau^2}{1+\omega^2\tau^2} \quad , \quad \varepsilon_2 = \frac{\omega_p^2\tau}{\omega(1+\omega^2\tau^2)}$$

On the other hand, ε for nonmagnetic materials can be expressed as[61,63]:

$$\varepsilon = \underline{n}^2 = (n + i\kappa)^2 = n^2 - \kappa^2 + i\,2n\kappa \qquad (3.4)$$

where $\underline{n}^2$ is the complex refractive index, and n is the real part; while κ, an imaginary part, is the extinction coefficient.

Combining equations (3.1) and (3.4) results:

$$n^2 = \frac{\sqrt{\varepsilon_1^2 + \varepsilon_2^2} + \varepsilon_1}{2}, \qquad \kappa^2 = \frac{\sqrt{\varepsilon_1^2 + \varepsilon_2^2} - \varepsilon_1}{2} \qquad (3.5)$$

Then, assuming that multiple reflection and interferences are negligible, the reflectivity at normal incidence can be determined by the relation[61]:

$$R = \frac{(n-1)^2 + \kappa^2}{(n+1)^2 + \kappa^2} \qquad (3.6)$$

With these expressions, the spectral reflectance can be obtained using the following parameters: ε_∞ and m^* for WO_3 films are 4.8 and $0.5m_0$ (m_0 is the free electron mass)[1,42]; and 3.85 and $0.3m_0$ for SnO_2 films[64], respectively. Figure 3.12 illustrates the calculated spectral reflectance of

polycrystalline electrochromic WO_3 films. The variables are the electron density n_e and mobility μ. It is observed that the onset of the reflectance shifts to lower wavelengths with increasing electron density (n_e). At low electron densities ($n_e < 10^{21}$ cm^{-3}), only little solar radiation is reflected. At high densities ($n_e > 3 \cdot 10^{21}$ cm^{-3}), an increasing amount of radiation is reflected so that the films appear strongly colored. The spectral reflectance is also dependent on the mobility. and the reflectance increases rapidly with an abrupt slope for higher mobilities μ. In order to obtain energy efficient control in windows, the onset of high reflectance should occur at $\sim \lambda = 0.8$ μm. Theoretically, it is expected that n_e should be about $5 \cdot 10^{21}$ cm^{-3} and μ as high as possible, preferably about 20 cm^2 /Vs.

Svensson *et al.*[1–3] had reported the theoretical reflectivity of polycrystalline electrochromic WO_3 based on the double injection model and the ideal ionized impurities scattering theory[1]. Their calculated spectral reflectance only depends on the electron density n_e, and their theoretical values were higher than the experimental values which had a much more graded onset (slow increase of reflectance). This difference was interpreted as a result of poor crystallinity.

Comparing with Svensson's model, the reflectance in the theoretical model presented above is also influenced by the mobility μ which is determined by collisions between electrons and phonons[63] and related to the crystallinities of films. A poor crystalline film has a much lower electron-mobility. The introduction of the mobility in reflectance spectra, in principle, will explain the dependence of film crystallinity on its reflectivity.

(2). Experimental Results

The phenomenon of blue coloration of WO_3 films has been investigated by various authors[8,15,28]. Investigations of the optical absorption of colored WO_3 films revealed a broad absorption band peaked at energies near 1.2 ~ 1.4 eV ($\lambda \cong 0.8 \sim 1$ μm) for amorphous films and 0.84 eV ($\lambda \cong 1.5$ μm) for crystalline films. The films appear blue as a results of absorption in the near infrared and visible red part of the solar spectrum. This absorption was believed to be attributed to an intervalence transfer between W^{5+} and W^{6+} sites[28]; and the states of penta-valent tungsten W^{5+} were formed by an injection of electrons into WO_3 from the cathode during coloration. In crystalline films, the injected electrons behave like free electrons which can be described by the Drude model[61].

Figure 3.13 illustrates the measured infrared reflectance spectra of as-prepared, colored and bleached WO_3 film deposited onto glass at 400°C with a thickness of 450 nm, and a theoretical calculated spectrum of the colored film from the Drude theory. The as-prepared WO_3 film exhibited no significant reflectivity other than some peaks due to an interference effect. After coloration, proton and electron insertions caused an increase in reflectivity of approximately 45% at wavenumbers smaller than 4000 cm^{-1}. The increase in reflectance for colored film is in agreement with results on evaporated and sputtered WO_3 films[12,15]. Cogan *et al.*[10] also investigated the reflectance in sputter-deposited thin films of crystalline Li_xWO_3 as a function of lithium concentration ($0<x<0.5$), and found that

the magnitude of the reflectance increased with increasing Li insertion to a concentration of Li_xWO_3 and the onset of reflectance moved to the shorter wavelength at higher lithium concentrations. These observations are in agreement with results predicted by the Drude theory.

Curve C in Figure 3.13 is the theoretical reflectance calculated from the equation (3.6) using $n_e = 1.9 \cdot 10^{21}$ cm^{-3} and $\mu = 2.5$ cm^2/Vs which were estimated by Hall measurements. The experimental values show a maximum deviation from the theoretical values of 10% at low wavenumbers (high wavelength). This is likely due to other scattering centers, such as impurities, defects, dislocations and grain boundaries, in the polycrystalline films, since these are important in poorly crystalline films.

After the film was bleached, the IR reflectance spectrum was measured (see curve D in Figure 3.13). It was found that the bleached film exhibits a similar reflectivity as the as-prepared film. This indicates that the optical properties of electrochromic WO_3 films are switchable between colored and bleached states. However, the somewhat higher reflectance of bleached film is believed to be a results of a small amounts of electrons and protons not being extracted and still staying in the film after bleaching.

Figure 3.14 shows the visible reflectance spectra of uncolored and colored films deposited at 350°C with a thickness of 400 nm. No significant reflectance change in visible region was observed after the sample was colored (Note: the peaks in the reflectance spectrum of uncolored film are due to the inteference effect). Figure 3.13 and 3.14 indicate that the infrared reflectance change is much more than visible reflectance because injected

electrons in a polycrystalline WO_3 film show near free-electron behavior. Therefore, the polycrystalline electrochromic WO_3 films exhibit infrared reflective modulation.

Figure 3.15 illustrates the infrared reflectances of two samples prepared at different substrate temperatures of 320°C and 400°C with a thickness of 550 nm and 450 nm respectively. It was found that the magnitude of reflectance of colored films (same coloration parameters) was quite dependent on the substrate temperature during deposition. As the substrate temperature increases, the infrared reflectance of the colored samples also increases. Because the films deposited at a higher temperature have a higher crystallinity, and a smaller density of grain boundaries, the electrons injected into such films show more likely free-electron behavior which results in higher reflectance.

Based on the reflectance measurements in Figure 3.13, it can be concluded that the colored polycrystalline WO_3 films exhibit near free-electron behavior although the experimental results did not fit the theoretical results very well. Thus the dielectric constant of the electrochromic WO_3 films can be treated by the Drude theory and reflectance of the films is then primarily determined by the density and scattering of the free electrons. Note, that the infrared reflective modulation theory based on the Drude model is not valid for amorphous films. Cogan *et al.*[10] investigated the optical properties of amorphous WO_3 films with Li insertion, and found that amorphous WO_3 films exhibit no evidence of a reflective component for Li insertion concentration up to x=0.4 in Li_xWO_3. Amorphous WO_3 is not expected to become reflective because the injected

electrons are located at optically absorbing bound states and are prevented from exhibiting free electron behavior. Thus amorphous WO_3 films display modulated absorption rather than modulated reflectance[1].

The infrared reflectance of SnO_2:F film was also investigated and the results are shown in Figure 3.16. The tin dioxide film has a high reflectance over a broad infrared range and has a high transmittance ~ 80% in visible spectrum[64,65]. The experiments have shown that fluorine-doped tin dioxide films exhibit metal-like behavior[64] which can be described by the Drude theory[61]. Using the measured values of the electron density $n_e = 4.6 \cdot 10^{20}$ cm^{-3} and the mobility $\mu = 14$ cm^2/Vs by Hall measurements, the infrared reflectance is theoretically predicted as illustrated in Figure 3.16. By comparing measured values of the reflectance with the theoretical values calculated from equation (3.6), it is found that the Drude model fits to the reflectance data in the near infrared region of SnO_2 films better than that of colored WO_3 films. This may be due to a difference in the effect of impurities, grain boundaries and surface effects etc. in SnO_2 and WO_3 films on reflectance. For SnO_2 films, the main impurities, such as Na atoms, diffuse from the soda glass substrate into the tin dioxide layer during the pyrolysis spray process[64]. The influence can be negligible if the concentration of sodium is small (<1%)[64]. However, for WO_3 films, influences from the impurities, neutral point defects, dislocations, grain boundaries and surface effects etc. is much more complex[1] such that the full validity of the free-electron Drude theory is questionable. A poor crystallinity of films will cause substantial deviation of experimental results from theoretical predictions. Therefore, it is

necessary to work out a modified Drude model to satisfactorily explain the complex scattering mechanism in the polycrystalline films.

Figure 3.17 illustrates the infrared reflectance of WO_3 film deposited onto SnO_2:F substrate at 400°C. The reflective property in this sample is substantially different from those of a single layer reflectance from WO_3 or SnO_2 films, since the multi-reflectance should be considered in this double layered structure. It was found that the average reflectance in the infrared region was increased for both uncolored and colored states. This is desirable for solar energy efficiency control, because almost 50% of the total solar energy comes as infrared radiation[1].

3.2.3 b) Transmittance Properties of EC Cells

Figure 3.18 shows the visible transmittance change of an electrochromic cell before and after coloration. The DC voltage applied to the working electrode and the counter electrode of the EC cell is –1.5 V. As shown in this figure, the transmittance reduced from 42% to 5% at a wavelength of $\lambda \approx 800$ nm when the EC cell was in the color state. It was found that after coloration the transmittance decrease in the visible red and near infrared region was more pronounced than in the visible blue region, which indicates an increase of the reflectance and (or) absorption in the visible red and near infrared region.

Figure 3.19 presents the time response of the EC cell. The relative transmittance of the white light decreased 50% within 200 seconds after a

bias of –1.5 V was applied to the EC cell (color state). When reversing the bias to +1.5 V, the transmittance increased and returned to a nearly initial clear state within 8 minutes. It was found that by shorting the circuit (0 V) the bleaching process could also be performed. However, a longer bleaching time was required to reach the same transmittance as with +1.5 V applied. The result is shown in Figure 3.19 (curve C). By removing the bias entirely the color state could remain unchanged for a certain time period depending on the choice of electrolytes and ambient conditions. It was reported that colored WO_3 films in solid state EC cells have a longer lifetime than in liquid electrolyte EC cells. On the other hand, liquid electrolyte EC cells can switch faster than solid state EC cells due to increased ionic mobility[5]. It was found that the lifetime of colored WO_3 films also is dependent on the ambient conditions. Generally, the persistance of the blue phase for colored samples stored in air ranged from days to weeks. Hurditch[27] observed no change in color for samples stored under vacuum over several months. Therefore, it is reasonable to believe that the lifetime or aging of the blue color will not change during measurements of the colored samples, even if the X-ray diffraction measurements took about 2 hours.

Table 3.1 Dependence of coloration time on thickness and deposition temperature of WO_3 films

Thickness (nm)	Deposition temp.(^0C)	Coloration time for entire area (sec.)	Resistivity (Ω.cm) uncolored	colored
300	350	40	30	0.012
450	350	60	35	0.016
600	350	120	51	0.026
450	250	80	2100	0.035
450	400	55	1.8	0.022

Table 3.2 XRD peak analysis of Fig. 10(a) & (b) for uncolored, colored and bleached WO_3 films deposited at 350 and 400 °C

Deposition temp. (°C)	Peak (2θ) ±0.05	I_a (uncolored)	I_b (colored)	Ratio I_a/I_b	I_c (bleached)	Ratio I_a/I_c
350	23.10	100.0	100.0	1.00	100.0	1.00
	23.60*	12.5	~	~	13.5	0.93
	24.30*	7.1	~	~	7.9	0.90
	27.85	4.8	6.6	0.74	5.5	0.89
	28.70	4.7	5.8	0.82	5.4	0.88
	33.40**	~	4.7	~	~	~
	47.20	6.0	5.8	1.03	5.7	1.04
	47.95**	~	3.8	~	~	~
	50.50	3.9	5.0	0.77	4.3	0.91
	53.60	2.7	3.2	0.82	3.0	0.90
400	23.10	100.0	100.0	1.00	100.0	1.00
	23.60*	13.3	~	~	10.5	1.25
	24.30*	5.4	~	~	4.4	1.22
	27.85	5.5	9.4	0.58	5.1	1.08
	33.30	15.7	50.7	0.31	19.4	0.81
	33.65*	16.7	~	~	20.1	0.83
	37.25	3.1	5.8	0.53	3.4	0.90
	47.20	6.5	5.9	1.10	5.6	1.15
	47.95**	~	7.1	~	~	~

Note: After films were colored, some peaks(*) disappeared and some new peaks(**) were observed. For other peaks, a little shift in the peak position was observed.

Table 3.3 The d-spacings and crystal planes for uncolored and colored WO_3 film deposited onto glass at 400 ^{0}C

Uncolored film (WO_3)				Colored film ($H_{0.23}WO_3$)			
Peak (2θ) ±0.05	(hkl)	d-spacing (Å) measured	theoret.*	Peak (2θ) ±0.05	(hkl)	d-spacing (Å) measured	theoret.*
23.10	(001)	3.847	3.846	23.00	(001)	3.863	3.881
23.60	(020)	3.767	3.765				
24.30	(200)	3.660	3.651				
27.85	(210)	3.201	3.247	28.15	(011)	3.167	3.116
33.30	(021)	2.688	2.690	33.40	(111)	2.680	2.677
33.65	(201)	2.661	2.648				
37.25	(300)	2.411	2.434	37.50	(210)	2.392	2.338
47.20	(002)	1.924	1.923	47.05	(002)	1.930	1.941
				47.95	(220)	1.895	1.848

* d-spacings are calculated from Miller indices (hkl) and lattice parameters[19,35].

Table 3.4 The d-spacings and crystal planes for uncolored and colored WO_3 film deposited onto SnO_2:F substrate at 400^0 C

Uncolored film (WO_3)				Colored film ($H_{0.23}WO_3$)			
Peak (2θ) ±0.05	(hkl)	d-spacing (Å) measured	theoret. *	Peak (2θ) ±0.05	(hkl)	d-spacing (Å) measured	theoret. *
23.10	(001)	3.847	3.846	22.90	(001)	3.880	3.881
23.60	(020)	3.767	3.765				
24.35	(200)	3.653	3.651				
28.90	(111)	3.087	3.085	28.60	(011)	3.118	3.116
34.05	(201)	2.632	2.648				
35.70	(121)	2.513	2.507				
41.90	(221)	2.154	2.144	41.45	(021)	2.176	2.168
47.20	(002)	1.924	1.923	46.70	(002)	1.943	1.941
48.45	(012)	1.877	1.863				
50.70	(112)	1.799	1.802	50.10	(012)	1.819	1.819
53.50	(022)	1.711	1.713	53.25	(112)	1.718	1.718
54.20	(202)	1.691	1.701	54.55	(221)	1.680	1.669
54.95	(122)	1.669	1.662				
55.70	(212)	1.649	1.654				

* d-spacings are calculated from Miller indices (hkl) and lattice parameters[19,35].

Figure 3.1 X-ray diffraction patterns of the WO_3 films prepared on glass substrates at different deposition temperatures: 250℃, 300℃, 350℃ and 400℃

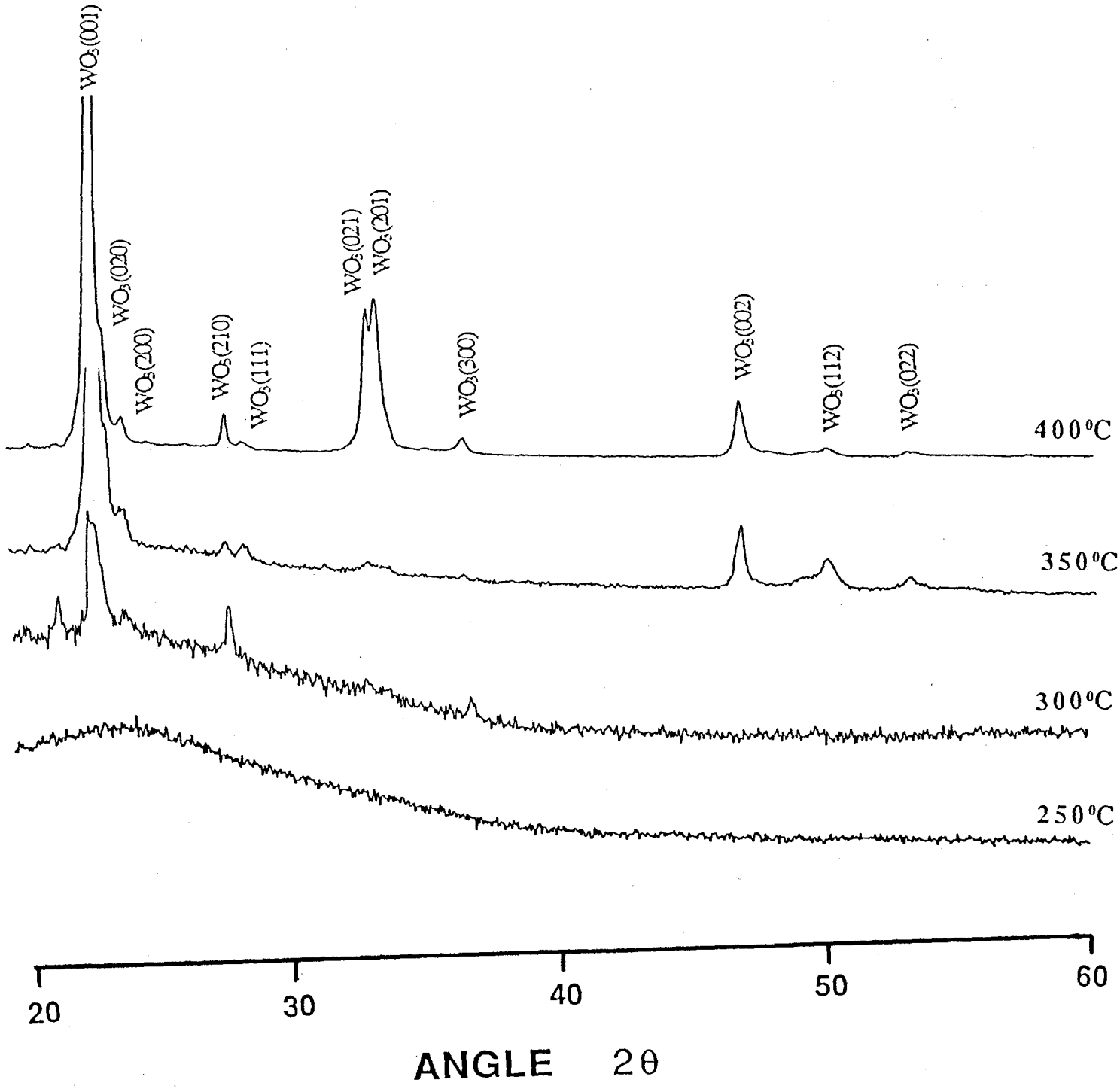
WO3(001)
WO3(020)
WO3(200)
WO3(210)
WO3(111)
WO3(021)
WO3(201)
WO3(300)
WO3(002)
WO3(112)
WO3(022)
400°C
350°C
300°C
250°C
20
30
40
50
60
ANGLE 2θ

Figure 3.2 X-ray diffraction patterns of

A): WO_3 film deposited onto the glass at 350°C

B): SnO_2:F film

C): WO_3 film deposited onto SnO_2:F substrate at 350°C

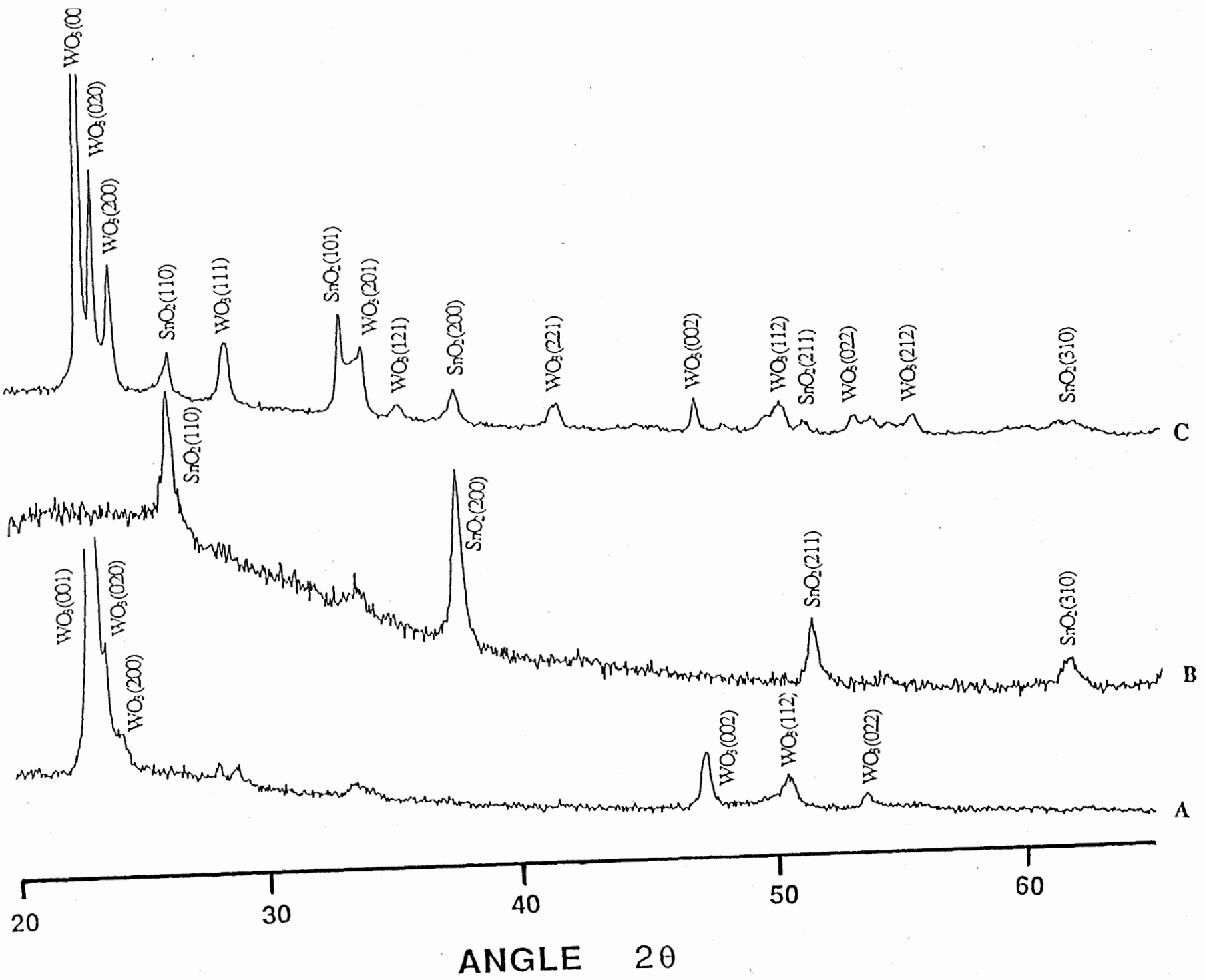
WO3(00
WO3(020)
WO3(200)
SnO2(110)
WO3(111)
SnO2(101)
WO3(201)
WO3(121)
SnO2(200)
WO3(221)
WO3(002)
WO3(112)
SnO2(211)
WO3(022)
WO3(212)
SnO2(310)
C
SnO2(110)
SnO2(200)
SnO2(211)
SnO2(310)
WO3(001)
WO3(020)
WO3(200)
B
WO3(002)
WO3(112)
WO3(022)
A
20
30
40
50
60
ANGLE 2θ

Figure 3.3 X-ray diffraction patterns of WO_3 films deposited onto SnO_2:F substrates at different temperatures:
250°C, 300°C and 400°C

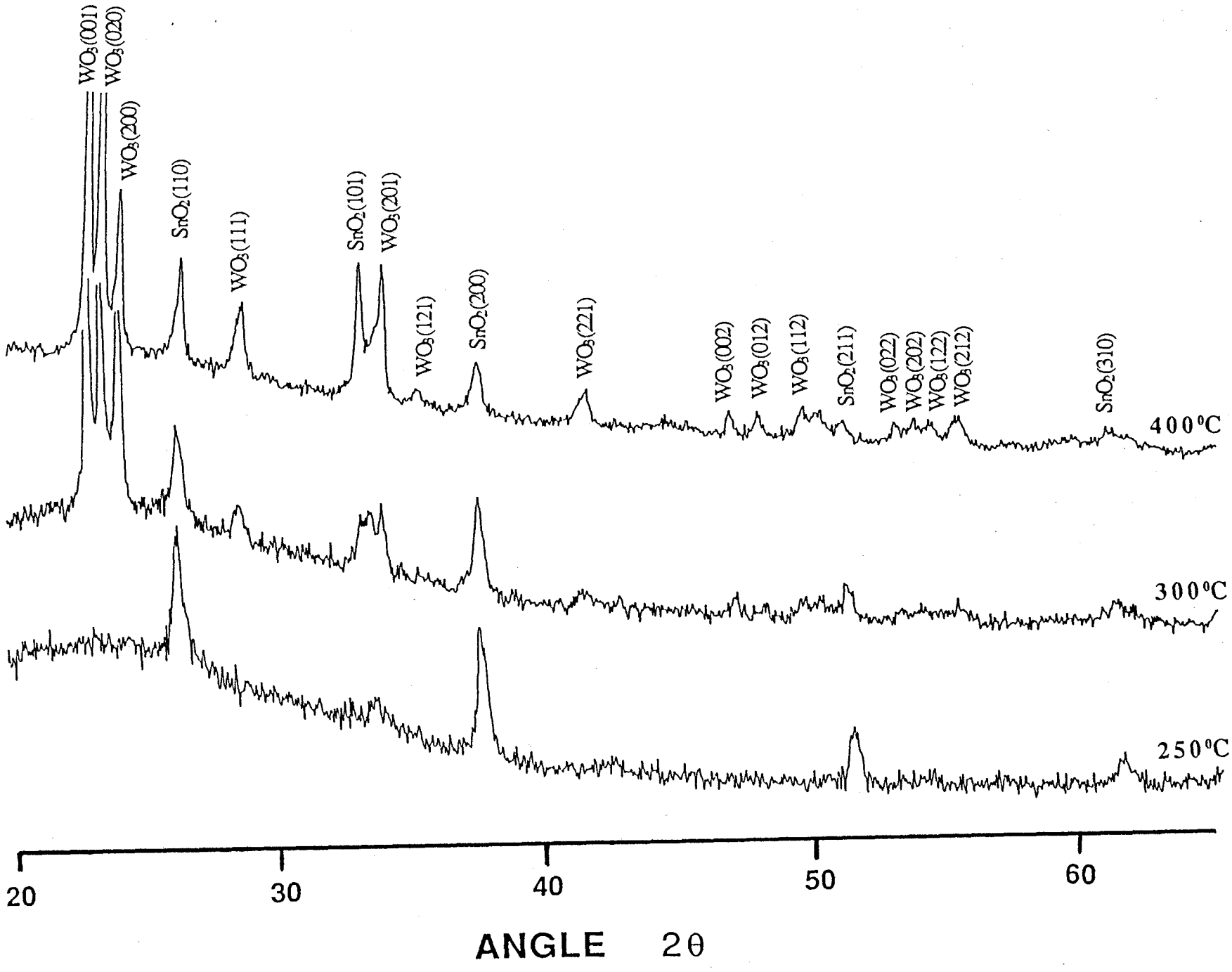
WO3(001)
WO3(020)
WO3(200)
SnO2(110)
WO3(111)
SnO2(101)
WO3(201)
WO3(121)
SnO2(200)
WO3(221)
WO3(002)
WO3(012)
WO3(112)
SnO2(211)
WO3(022)
WO3(202)
WO3(122)
WO3(212)
SnO2(310)
400°C
300°C
250°C
20
30
40
50
60
ANGLE 2θ

Figure 3.4 Dependence of the resistivity of the as-prepared WO_3 films with a thickness of 400 — 500 nm on the deposition temperature (substrate temperature)

Curve B is from Miyake *et al.*[6] on vacuum evaporated WO_3 films.

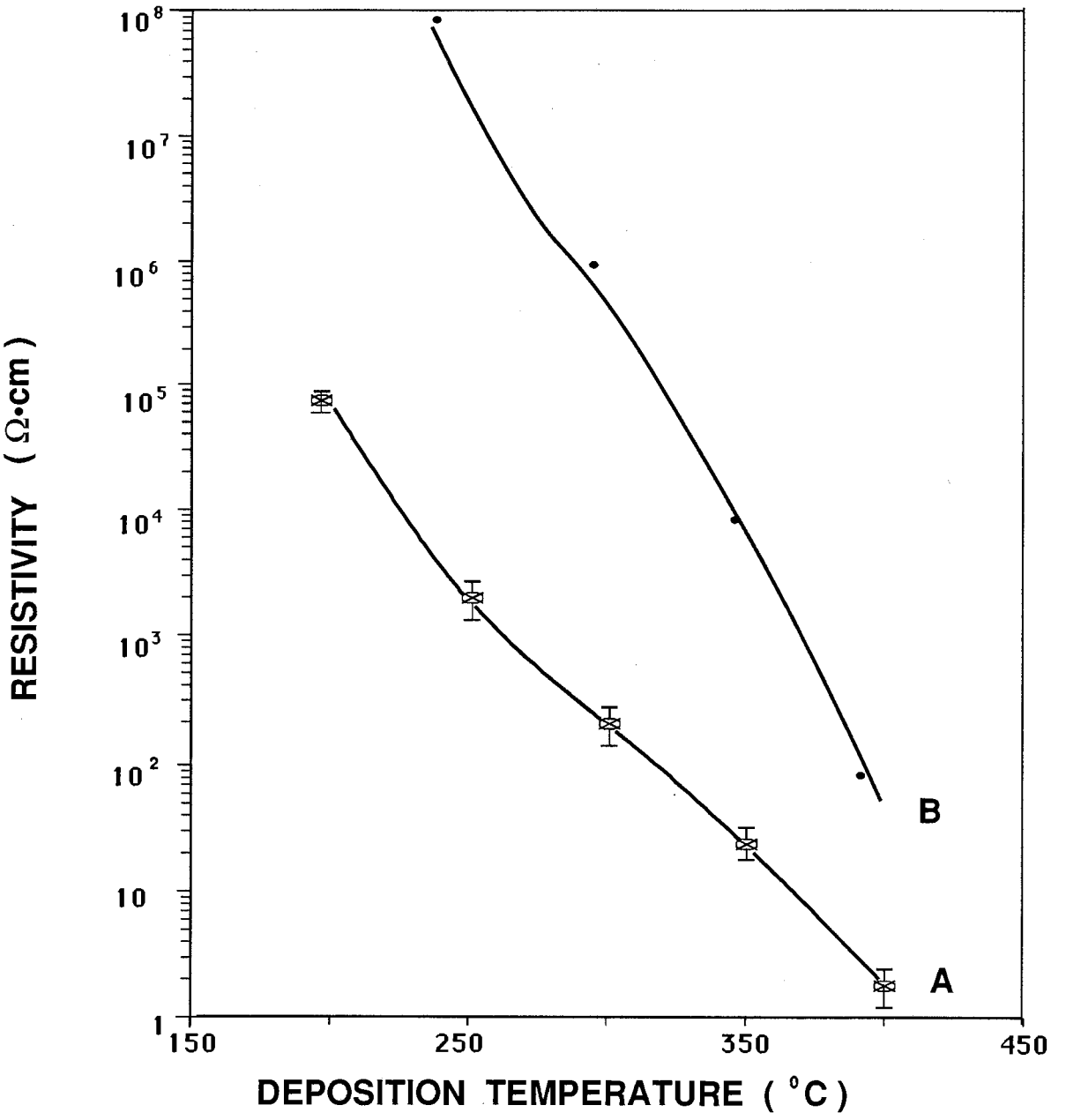
RESISTIVITY (Ω•cm)
10^8
10^7
10^6
10^5
10^4
10^3
10^2
10
1
150
250
350
450
DEPOSITION TEMPERATURE (°C)
B
A

Figure 3.5 Dependence of the resistivity of

A) uncolored

B) colored WO_3 films

on the deposition temperature

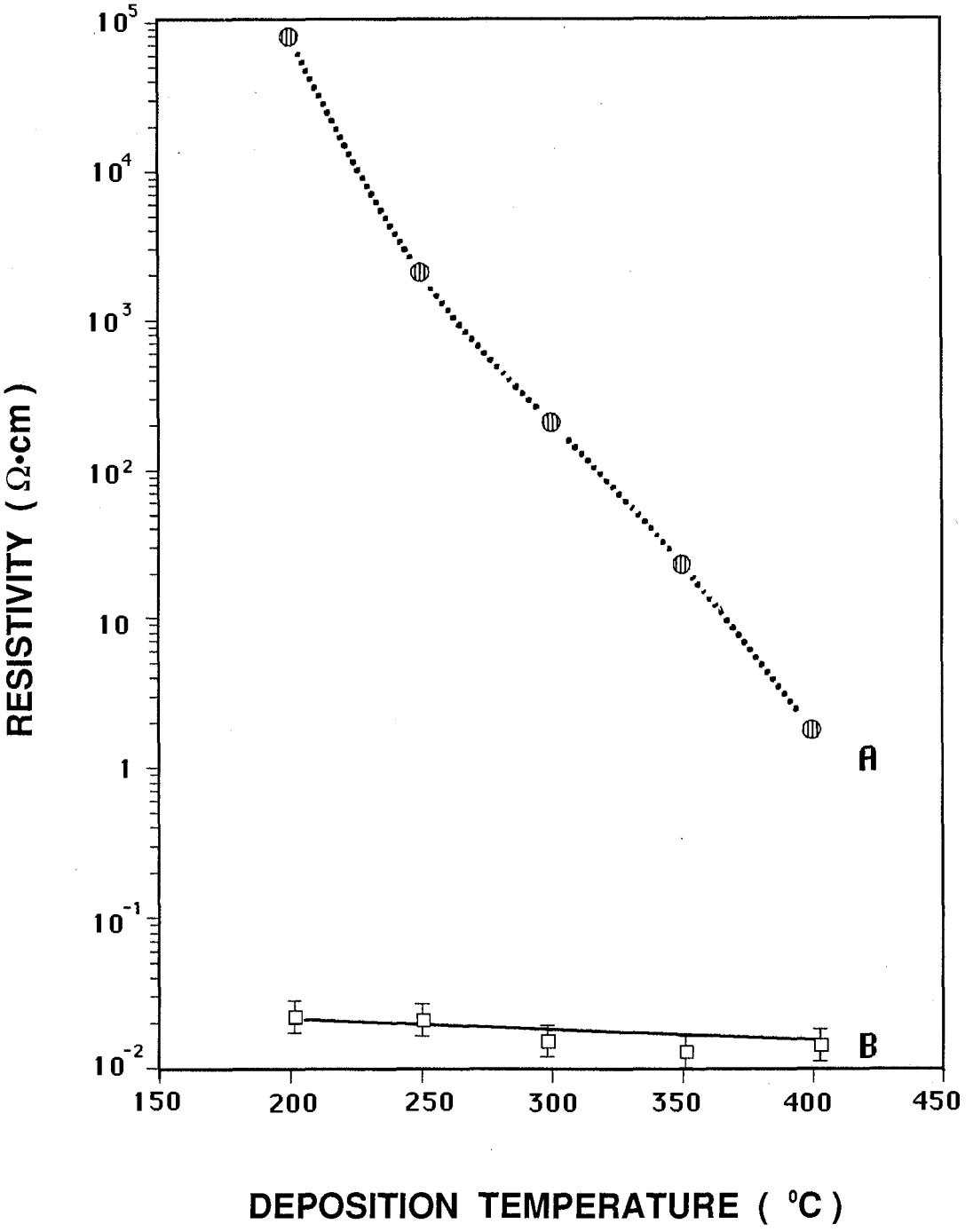
RESISTIVITY (Ω•cm)
10^5
10^4
10^3
10^2
10
1
10^-1
10^-2
150
200
250
300
350
400
450
A
B
DEPOSITION TEMPERATURE (°C)

Figure 3.6 Dependence of the resistivity (dotted line) and the carrier concentration (solid line) of colored WO_3 films prepared at 350℃ on the film thickness

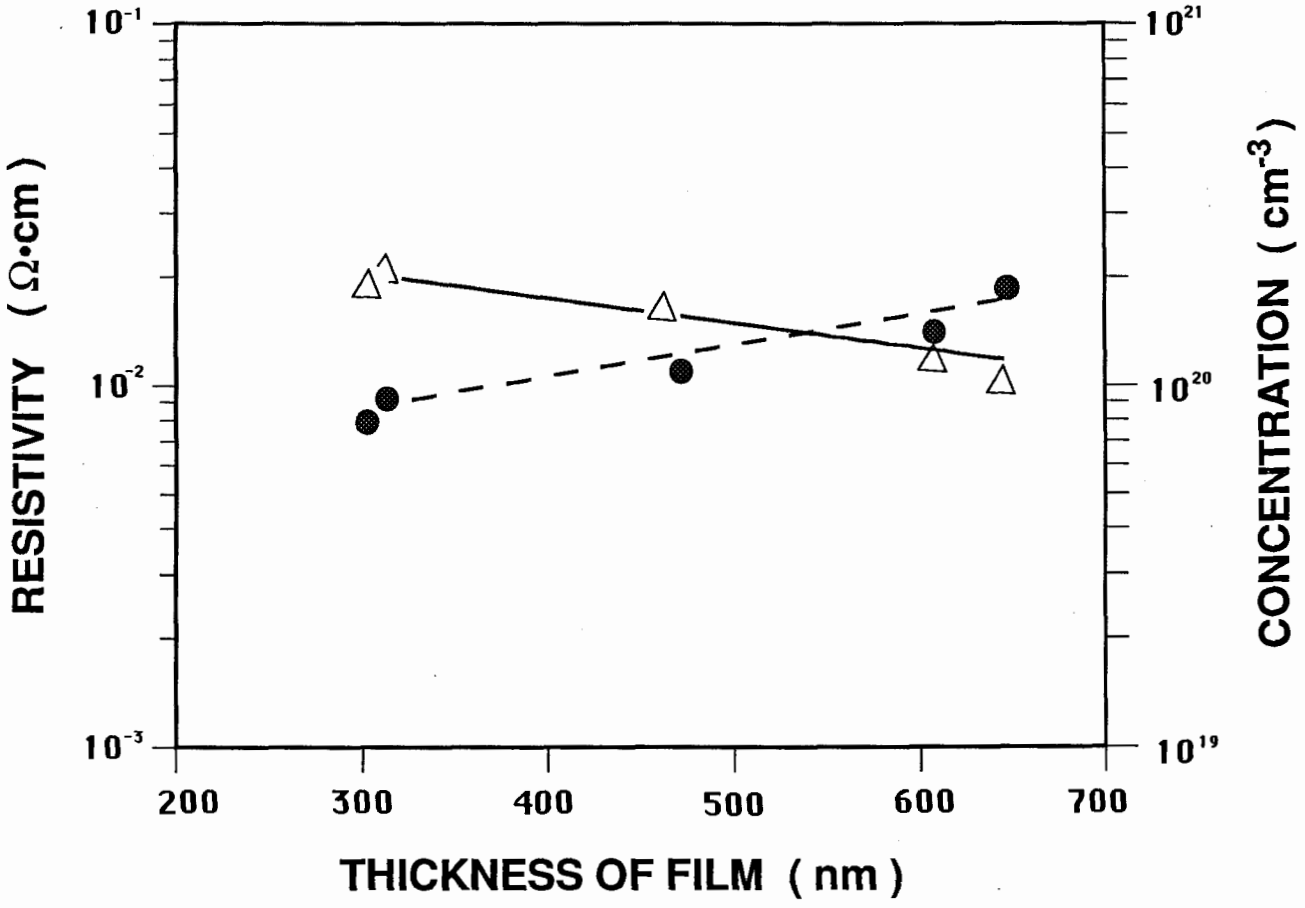
RESISTIVITY (Ω•cm)
CONCENTRATION (cm-3)
THICKNESS OF FILM (nm)
10-1
10-2
10-3
1021
1020
1019
200
300
400
500
600
700

Figure 3.7 Time dependence of the resistivity (circles) and the carrier concentration (squares) for WO_3 films prepared at 250℃ (dotted lines) and 350℃ (solid lines)

RESISTIVITY (Ω•cm)
0.001
0.01
0.1
1
0
2
4
6
8
10
TIME (minutes)
10^{18}
10^{19}
10^{20}
10^{21}
10^{22}
CONCENTRATION (cm^{-3})

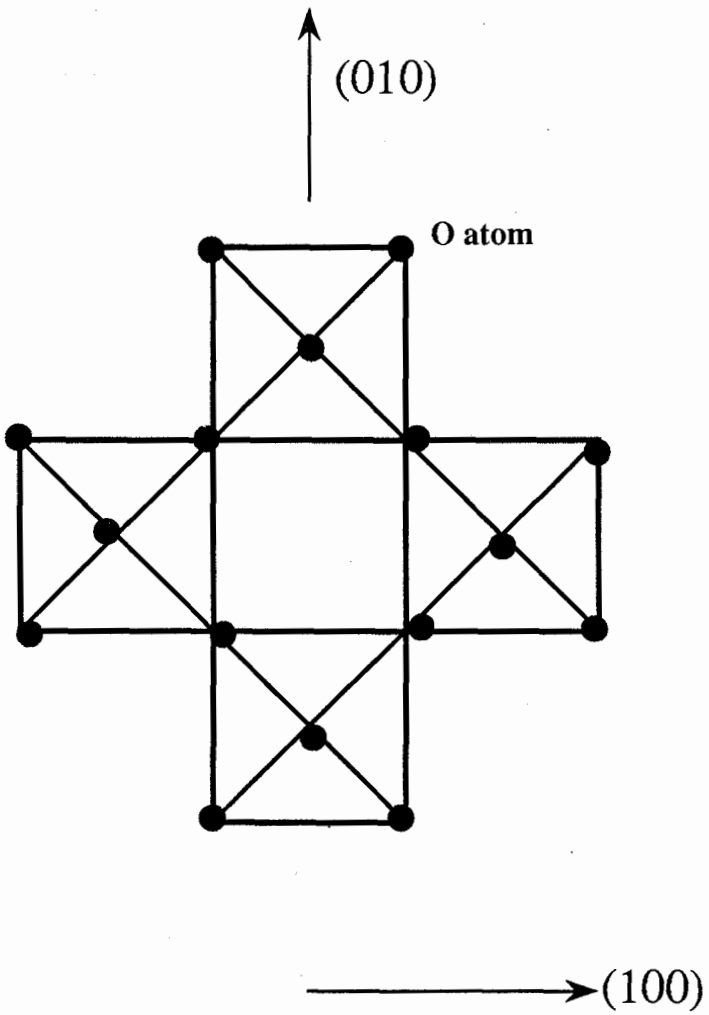

Figure 3.8 The skeleton illustrating a hollow channel in the (001) direction extending through the WO_3 structure

Figure 3.9 X-ray diffraction patterns of the WO_3 film prepared at 250°C for

A) uncolored film

B) colored film

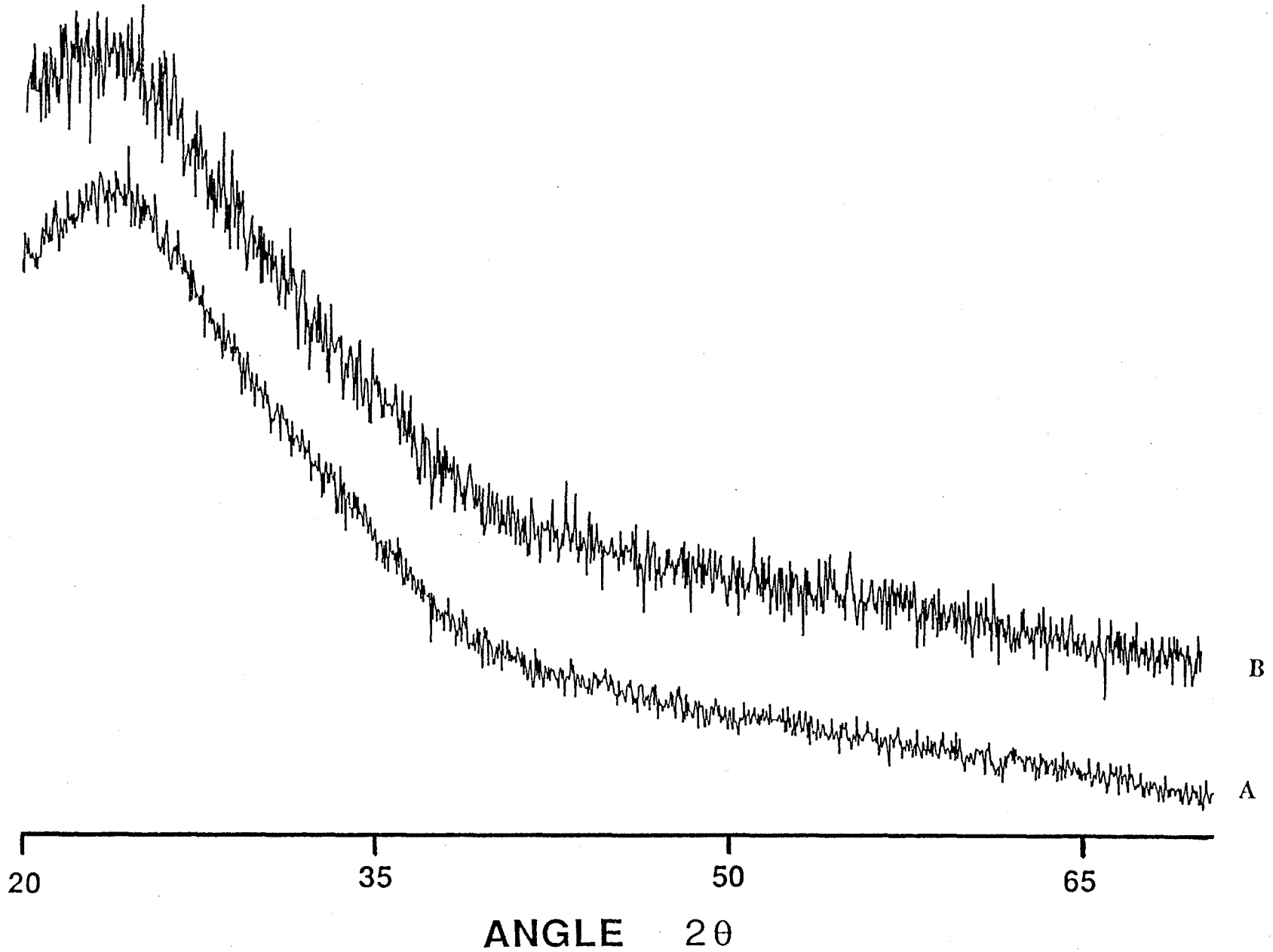
B
A
20
35
50
65
ANGLE 2θ

Figure 3.10 a) X-ray diffraction patterns showing the structural changes during the electrochromic process in WO_3 film prepared on glass at 350°C for

A) original (uncolored) film

B) colored film

C) bleached film

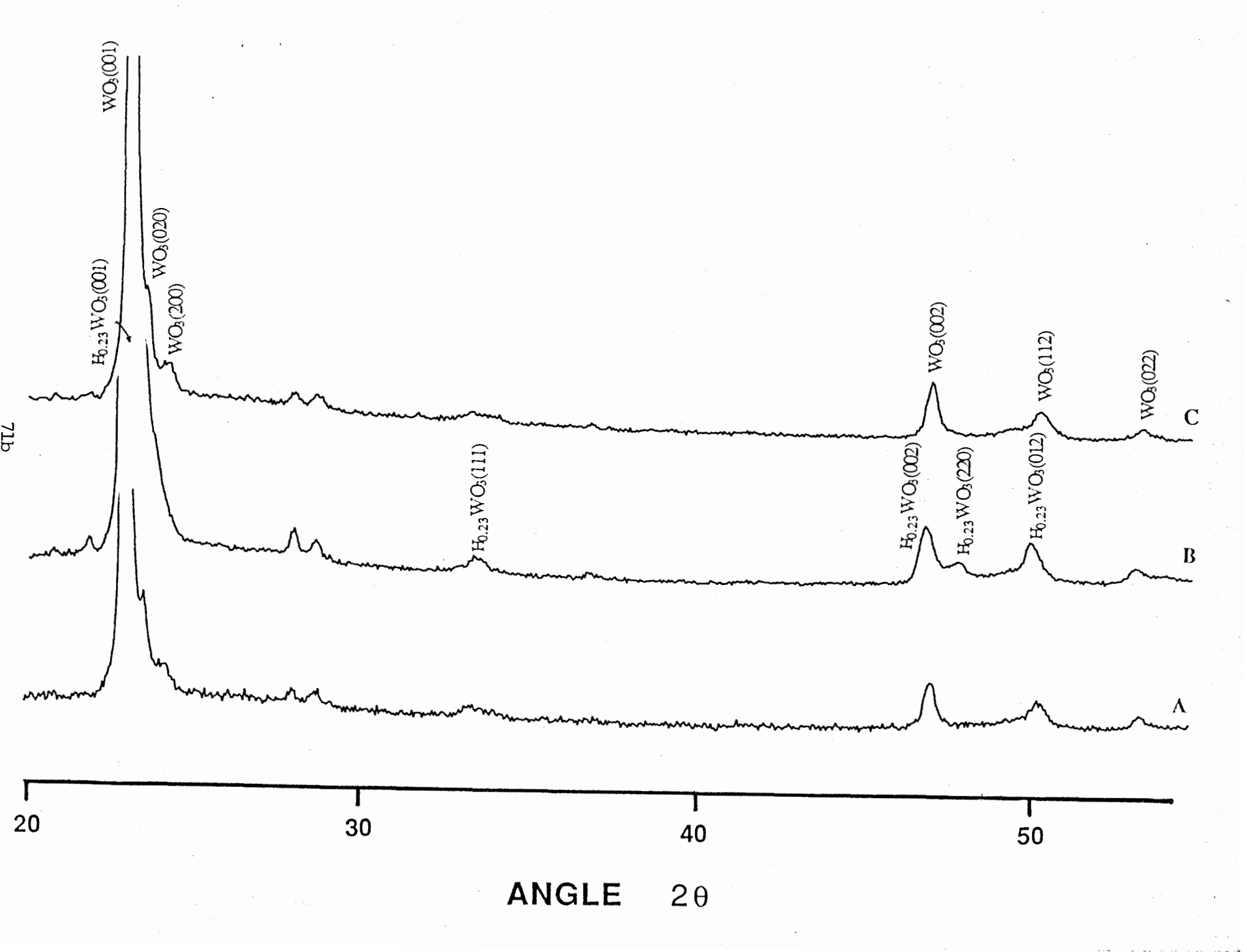
WO3(001)
H0.23WO3(001)
WO3(020)
WO3(200)
WO3(002)
WO3(112)
WO3(022)
C
H0.23WO3(111)
H0.23WO3(002)
H0.23WO3(220)
H0.23WO3(012)
B
A
20
30
40
50
ANGLE 2θ

Figure 3.10 b) X-ray diffraction patterns showing the structural changes during the electrochromic process in WO_3 film prepared on glass at 400℃ for

A) original film

B) colored film

C) bleached film

D) lighted recolored (light blue) film

E) strongly recolored (deep blue) film

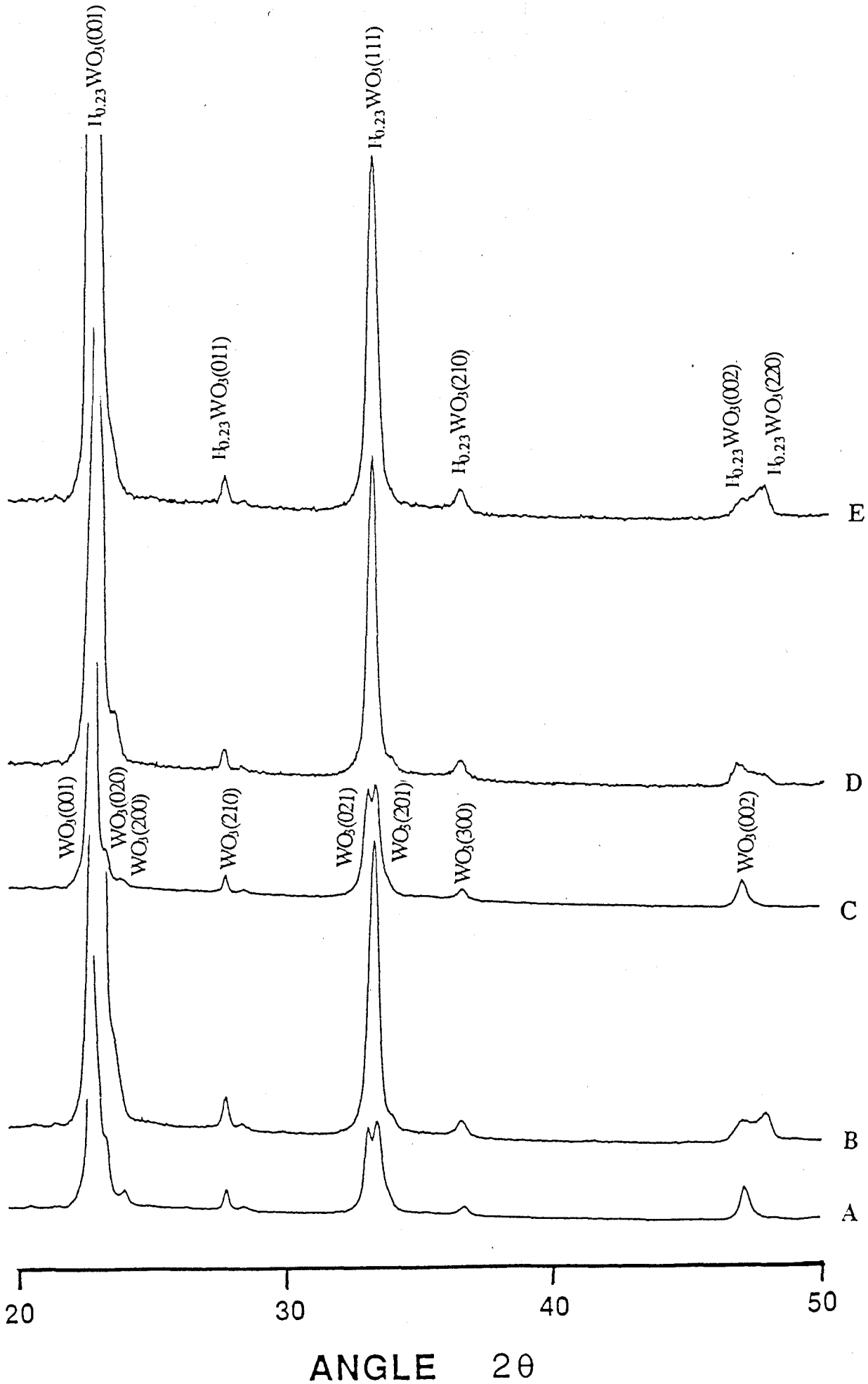
$H_{0.23}WO_3(001)$
$H_{0.23}WO_3(111)$
$H_{0.23}WO_3(011)$
$H_{0.23}WO_3(210)$
$H_{0.23}WO_3(002)$
$H_{0.23}WO_3(220)$
E
$WO_3(001)$
$WO_3(020)$
$WO_3(200)$
$WO_3(210)$
$WO_3(021)$
$WO_3(201)$
$WO_3(300)$
$WO_3(002)$
D
C
B
A
20
30
40
50
ANGLE 2θ

Figure 3.11 X-ray diffraction patterns showing the structural changes during the electrochromic process in WO_3 film prepared on SnO_2:F substrate at 400°C for

A) original film

B) colored film

C) bleached film

20
35
50
65
ANGLE 2θ
A
B
C
H0.23WO3(001)
WO3(001)
WO3(020)
WO3(200)
SnO2(110)
SnO2(110)
WO3(111)
H0.23WO3(011)
SnO2(101)
SnO2(101)
WO3(201)
WO3(121)
SnO2(200)
SnO2(200)
H0.23WO3(021)
WO3(221)
H0.23WO3(002)
WO3(002)
WO3(012)
H0.23WO3(012)
WO3(112)
SnO2(211)
SnO2(211)
WO3(022)
H0.23WO3(112)
WO3(202)
WO3(122)
H0.23WO3(221)
WO3(212)
SnO2(310)
SnO2(310)

Figure 3.12 Reflectances of the electrochromic WO_3 layer with different electron densities n_e ($\cdot 10^{21}$ cm^3) and mobilities μ (cm^2/Vs) computed from the Drude theory

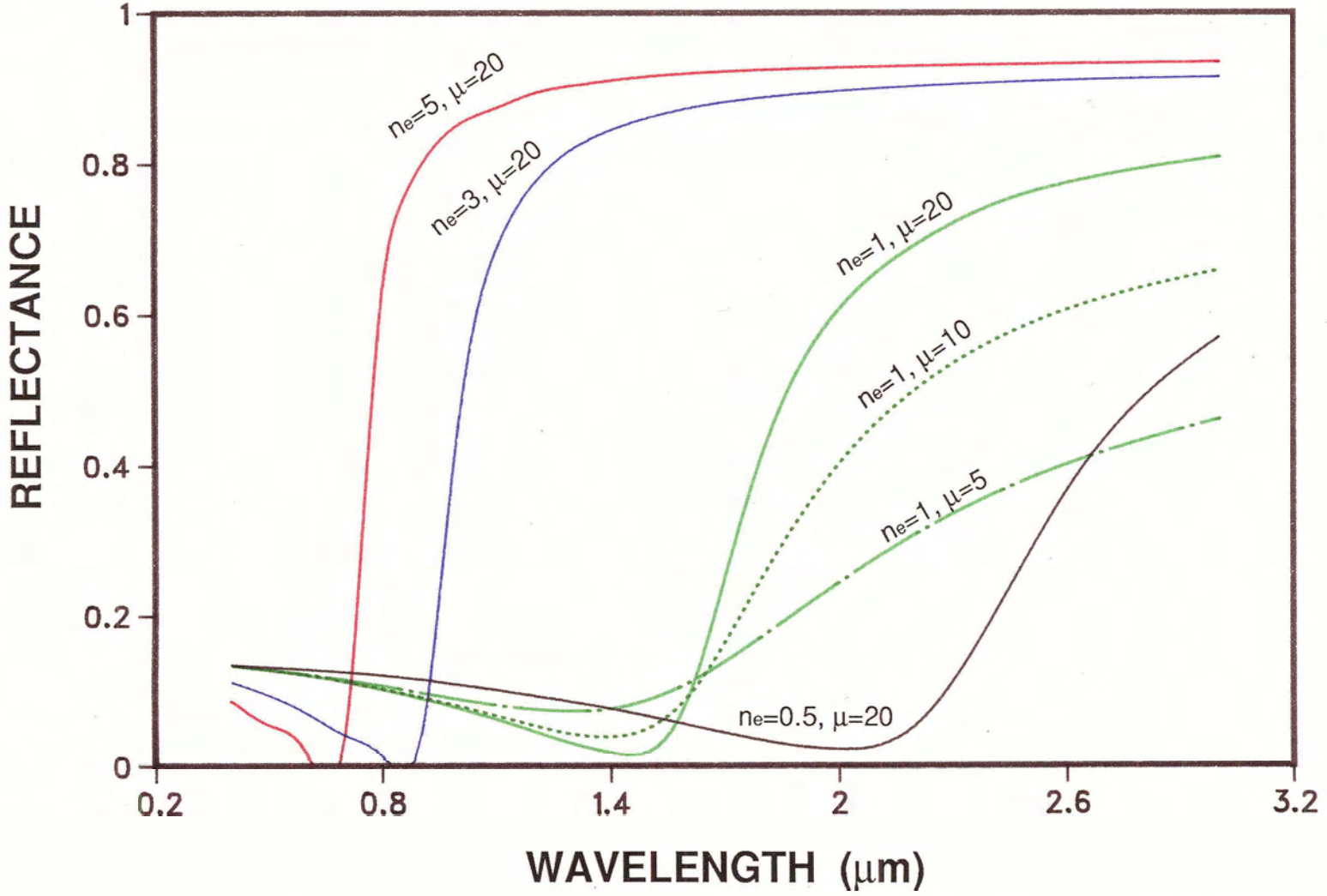
REFLECTANCE
WAVELENGTH (μm)
1
0.8
0.6
0.4
0.2
0
0.2
0.8
1.4
2
2.6
3.2
ne=5, μ=20
ne=3, μ=20
ne=1, μ=20
ne=1, μ=10
ne=1, μ=5
ne=0.5, μ=20

Figure 3.13 The measured infrared spectral reflectances of WO_3 film deposited at 400°C with a thickness of 450 nm for

A) uncolored film

B) colored film

D) bleached film

Curve C represents the calculated infrared spectral reflectance of the colored film using $n_e = 1.9 \cdot 10^{21}$ cm^{-3} , $\mu = 2.5$ cm^2/Vs, and curve E taken from Ref. [15] is the reflectance for a colored film prepared by evaporation and crystallized by thermal annealing.

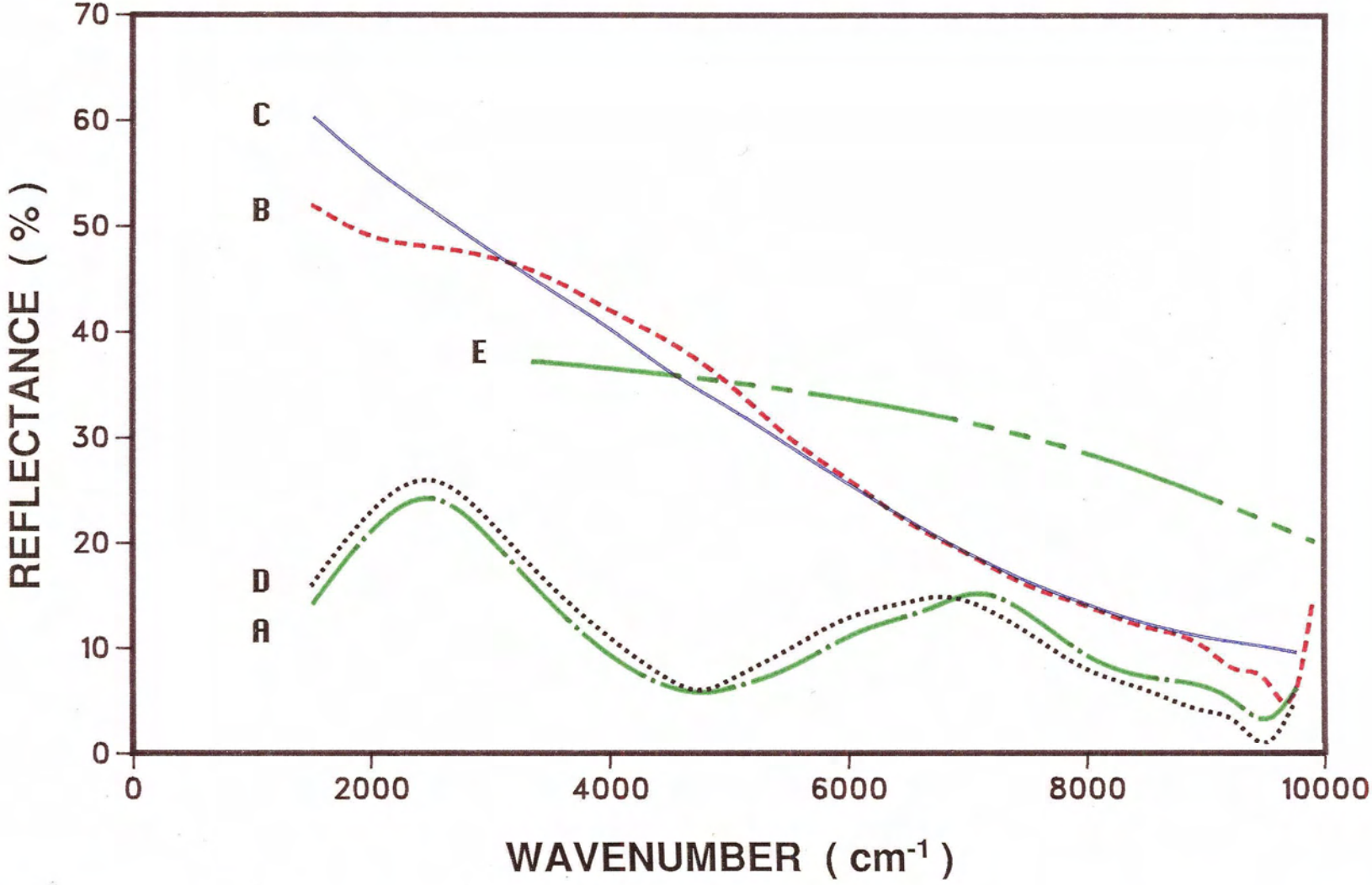
70
60
50
40
30
20
10
0
REFLECTANCE (%)
C
B
E
D
A
0
2000
4000
6000
8000
10000
WAVENUMBER (cm-1)

Figure 3.14 The measured visible spectral reflectances of WO_3 film deposited at 400°C with a thickness of 400 nm for

A) uncolored film

B) colored film

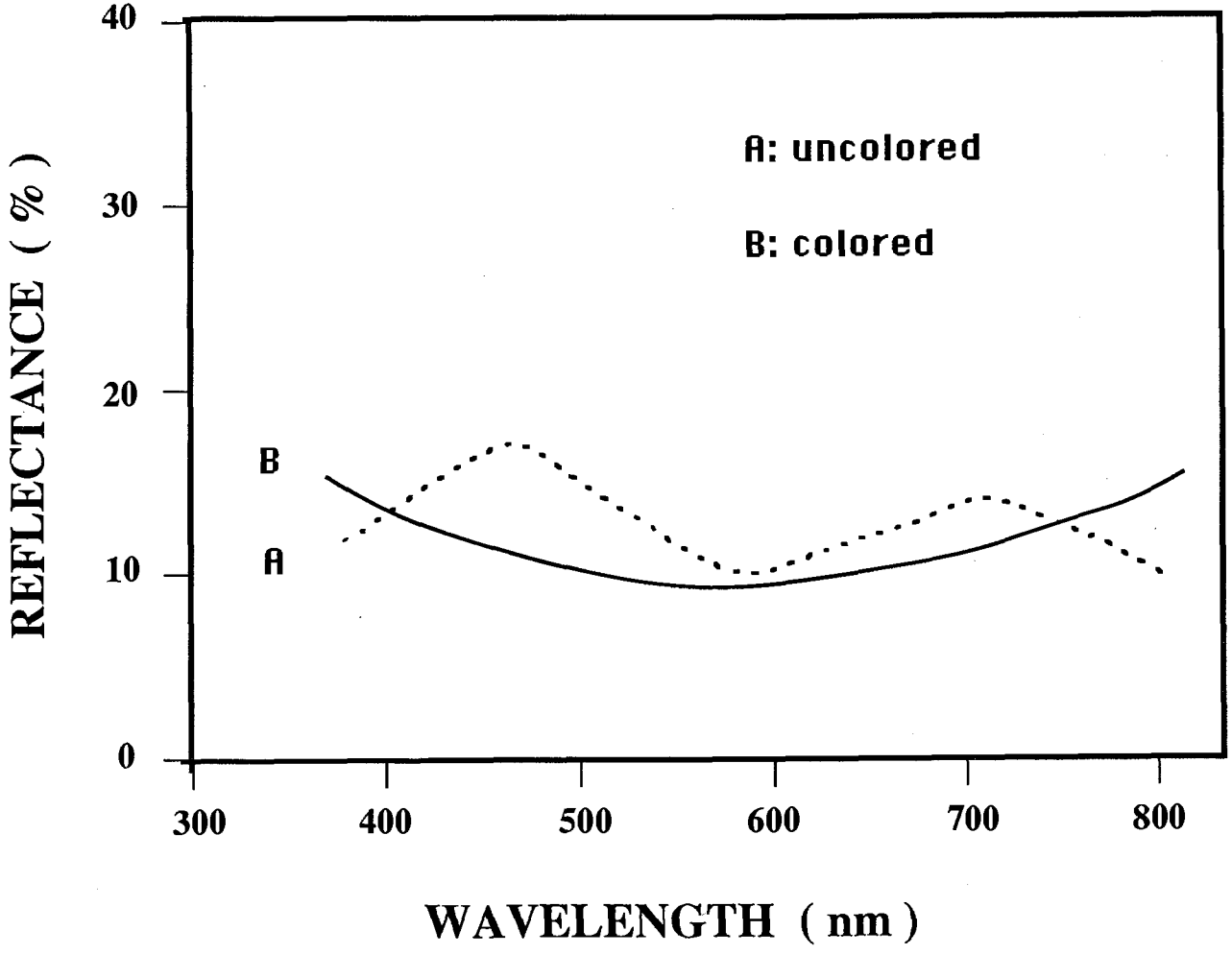
40
30
20
10
0
REFLECTANCE (%)
A: uncolored
B: colored
B
A
300
400
500
600
700
800
WAVELENGTH (nm)

Figure 3.15 The measured infrared spectral reflectances of

A) uncolored D) colored WO_3 films deposited at 400°C with a thickness of 450 nm

B) uncolored C) colored WO_3 film deposited at 320°C with a thickness of 550 nm

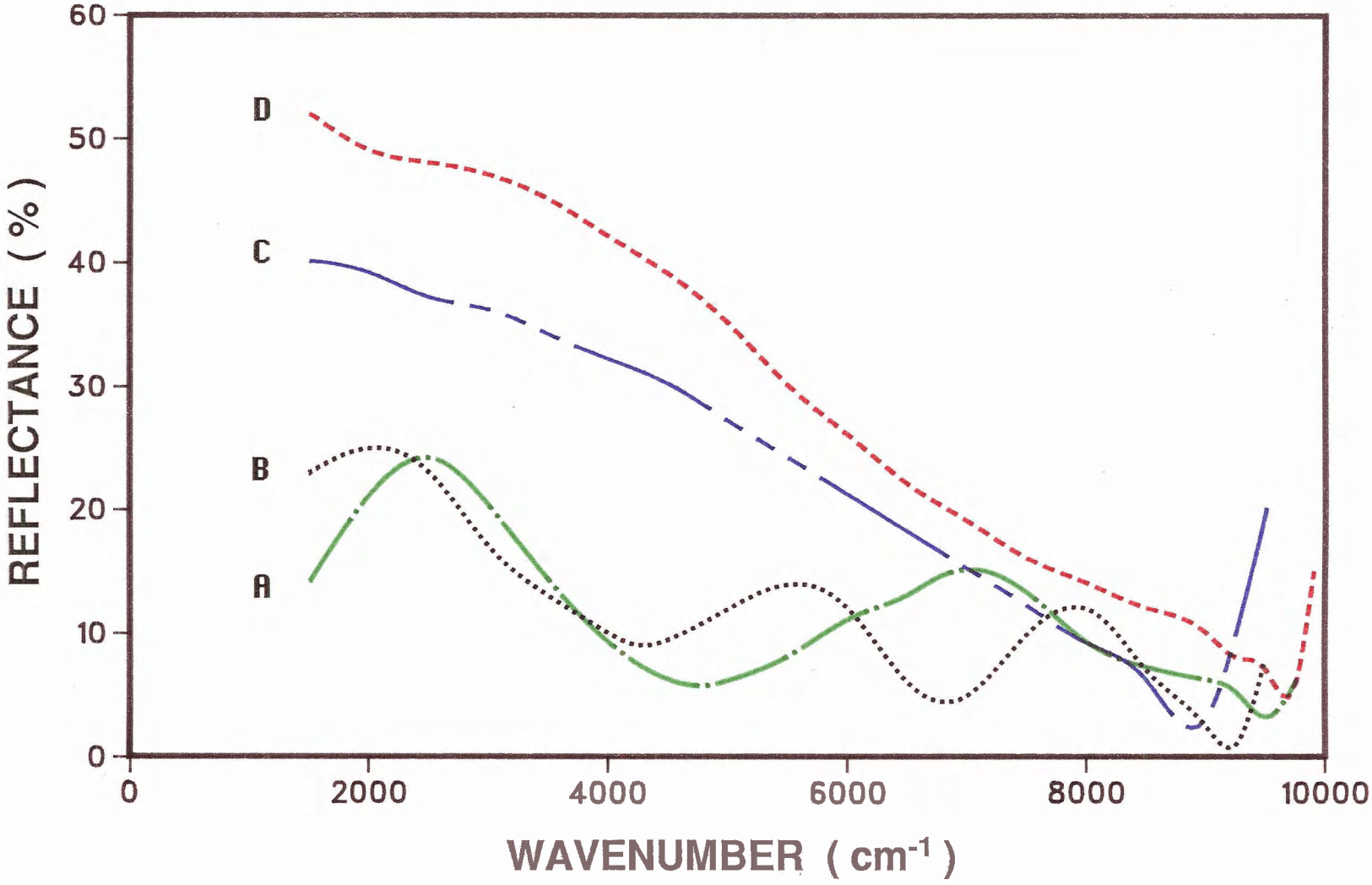
60
50
40
30
20
10
0
REFLECTANCE (%)
D
C
B
A
0
2000
4000
6000
8000
10000
WAVENUMBER (cm-1)

Figure 3.16 The calculated (dash line) and the measured (solid line) infrared reflectance spectra of SnO_2:F film with a thickness of 220 nm

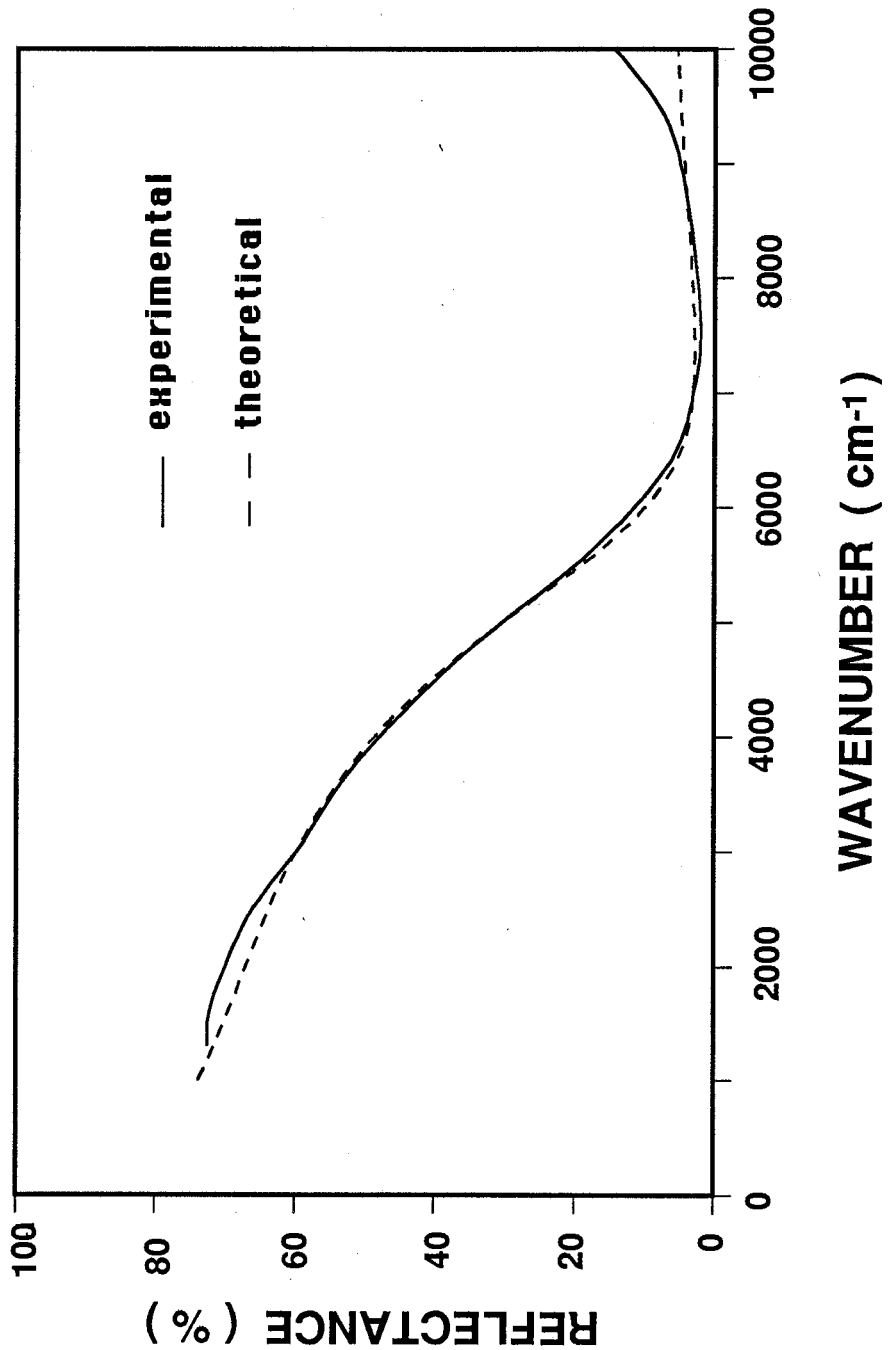
experimental
theoretical
REFLECTANCE (%)
100
80
60
40
20
0
0
2000
4000
6000
8000
10000
WAVENUMBER (cm-1)

Figure 3.17 The measured infrared reflectance spectra of WO_3 film with a thickness of 400 nm deposited onto SnO_2:F substrate at 400°C for

A) uncolored film

B) colored film

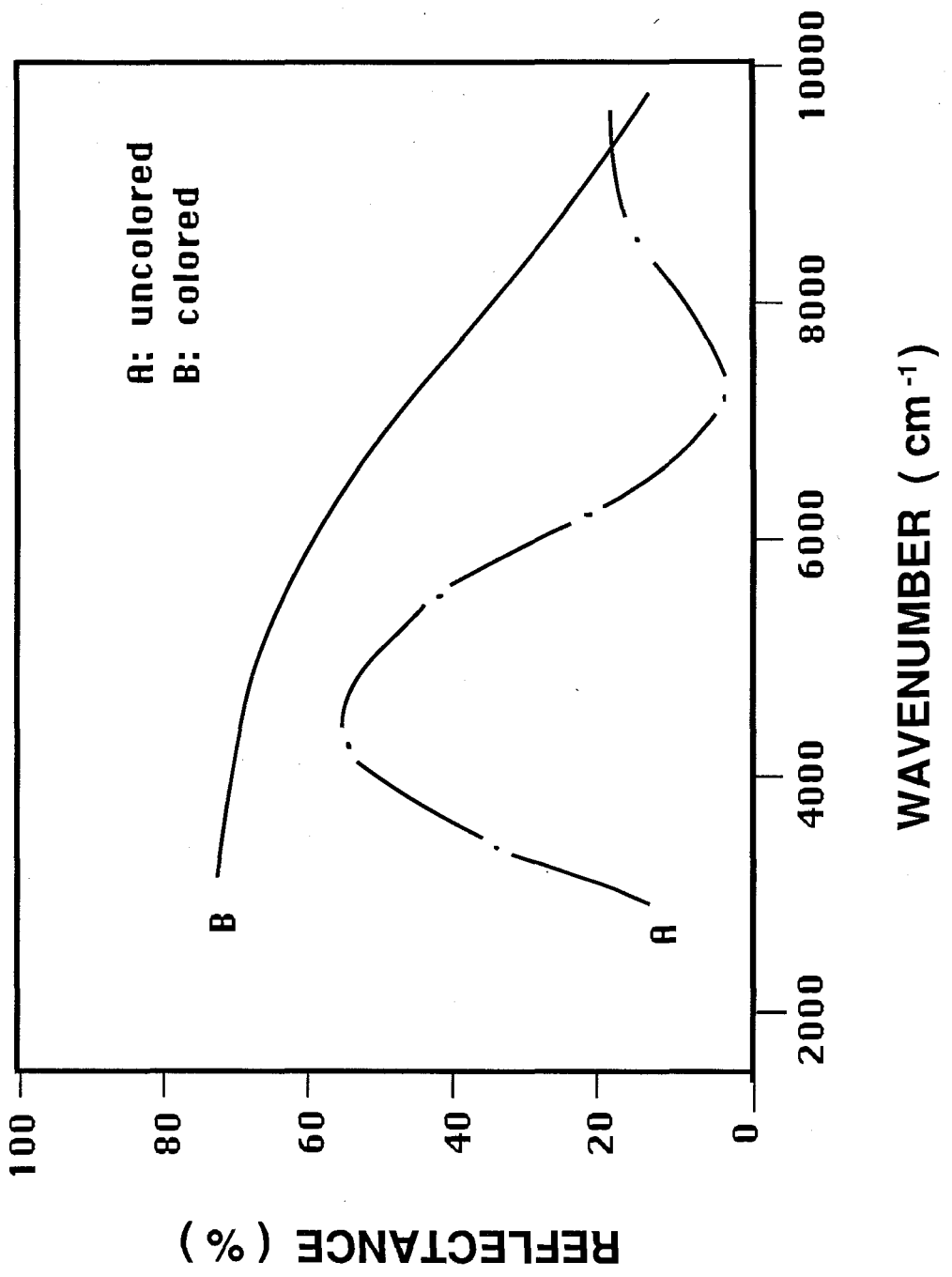
A: uncolored
B: colored
B
A
100
80
60
40
20
0
REFLECTANCE (%)
2000
4000
6000
8000
10000
WAVENUMBER (cm-1)

Figure 3.18 The visible transmittance change of the electrochromic cell before and after coloration

A) uncolored state

B) colored state

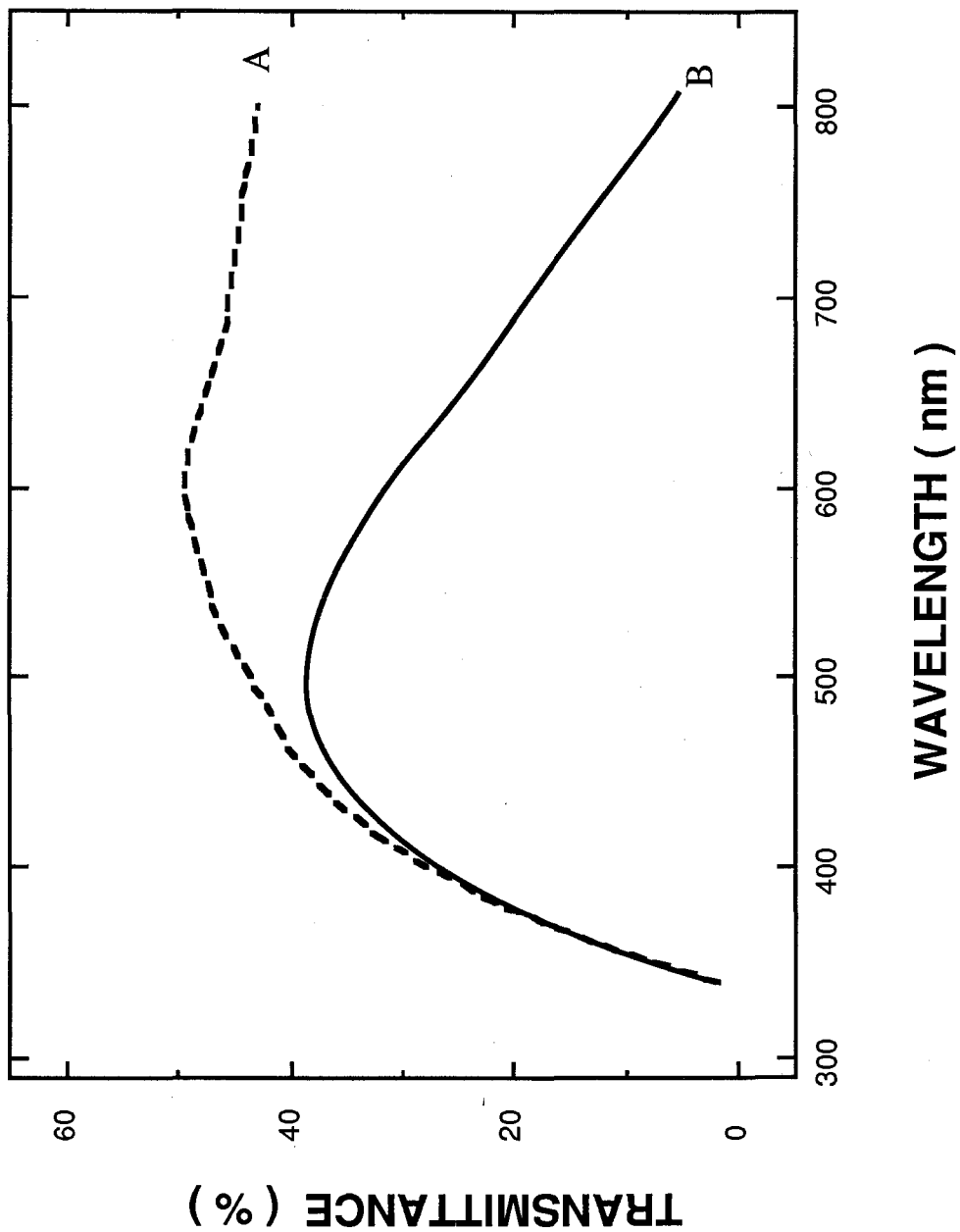
A
B
TRANSMITTANCE (%)
0
20
40
60
300
400
500
600
700
800
WAVELENGTH (nm)

Figure 3.19 Time response of the electrochromic cell

A) coloring process with –1.5 v applied

B) bleaching process with +1.5 v applied

C) bleaching process with shorting circuit (0 V)

D) remaining color state with open circuit

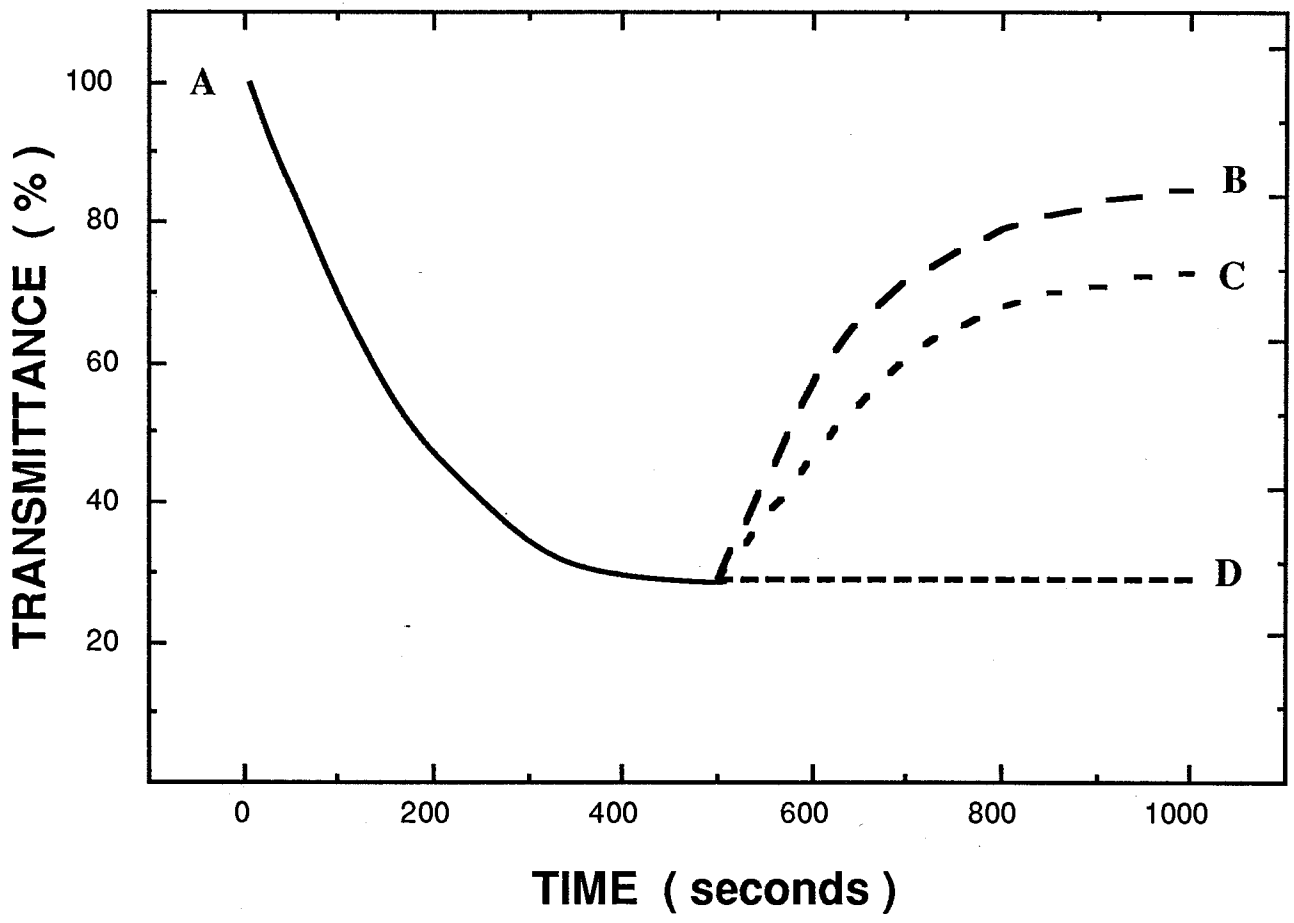
TRANSMITTANCE (%)
100
80
60
40
20
A
B
C
D
0
200
400
600
800
1000
TIME (seconds)

Chapter 4

SUMMARY AND CONCLUSIONS

The crystallinity and the resistivity of pyrolytically spray deposited tungsten trioxide films strongly depend on the substrate temperature during deposition. X-ray diffraction (XRD) patterns revealed that the WO_3 films deposited at temperatures above 300°C were polycrystalline in nature while those deposited below 300°C were amorphous. Many more diffraction peaks were observed in the diffraction patterns of the films deposited at the temperature of 400°C. The resistivities of the films deposited at substrate temperatures between 200°C and 400°C were found to be on the orders of 10^5 – 1 Ω·cm and decreased with increasing deposition temperature.

Electrochemically colored WO_3 films were investigated, and results revealed large variations in the electrical, optical and structural properties.

The resistivities of WO_3 films decreased by 2 ~ 8 orders of magnitude after coloration, and the carrier concentrations of the colored samples were estimated to be about 10^{21} cm^{-3} as determined by Hall measurements. The increase in the electrical conductivity of the colored films is believed to be due to the injection of both, a large number of electrons from the cathode and of protons from the electrolyte into WO_3 films. The resistivities of as-prepared amorphous WO_3 films were generally several orders of

magnitude higher than the resistivities of polycrystalline films depending on the deposition temperature. After coloration the resistivities of both, amorphous and polycrystalline films, reduced to approximately the same order of magnitude and seemed to be independent of the deposition temperature.

It was found that the resistivities of the uncolored and colored WO_3 films are essentially independent of the film thickness for films thicker than 200 nm. However, a longer coloration time would be required for the thicker films since thicker samples possess a larger volume space for intercalation.

The investigation on the coloration time dependence of the resistivity and the concentration of colored WO_3 films showed that the concentration and the conductivity of the polycrystalline samples increased rapidly within 1 – 2 minutes, and reached a plateau after about 6 minutes, while the concentration of amorphous films had a higher plateau than the polycrystalline films, and plateau was reached more slowly. This is likely due to the structure disparity between the polycrystalline and amorphous samples. The polycrystalline films have some channels allowing the electrons to diffuse easily into the crystal structure, while amorphous films are more porous, and have a large number of grain boundaries and a disordered structure, which can accommodate more electrons and protons.

X-ray diffraction studies revealed the structural changes of the polycrystalline WO_3 films during the electrochromic process. Some diffraction peaks were not observed and some new peaks appeared after the samples were colored. The diffraction peaks of the colored films could be

assigned to the planes of the hydrogen tungsten bronze $H_{0.23}WO_3$. The formation of the tungsten bronze is believed to be a result of the double injection of the electrons and protons into the WO_3 films. After the samples were bleached, the X-ray diffraction patterns changed to the original uncolored states. It is concluded that the crystal structure transforms from the tungsten trioxide to the hydrogen tungsten bronze during the coloration, and reverses from the hydrogen tungsten bronze to the tungsten trioxide during the bleaching.

The colored polycrystalline WO_3 films exhibit a free electron-like behavior. Their optical properties can be predicted by the Drude theory. According to this model, the infrared spectral reflectance is primarily determined by the density and the scattering of the free electrons. The measured infrared reflectance spectrum showed some deviation from the theoretical results. This likely arises from scattering centers other than ion scattering, such as impurities, defects and grain boundaries, included in the polycrystalline films. These scattering centers will become important for poorly crystalline films. The infrared reflectance measurements of the samples prepared at different substrate temperatures showed a higher infrared reflectance for the colored sample prepared at a high temperature (400℃), since the film has the better crystallinity and less grain boundaries than films prepared at lower temperatures. The electrons injected into such a film show more likely free electron behavior which results in a higher reflectance.

The performance of the electrochromic cells showed a visible transmittance change from 42% to 5% at the wavelength of 800 nm after

coloration. The time response of the EC cells revealed that the transmittance is switchable between colored and uncolored states which is very desirable for the "smart windows" application.

It was reported that some companies[66] are working on the developments of electrochromic coatings, such as, watches with electrochromic displays, electrochromic sun roof for automobiles, electrochromic rear-view mirror for motorcars, smart windows for buildings and greenhouses. However, these products have not been commercialized due to the difficulties of large-scale manufacturing techniques and high-cost manufacturing processes etc.. It will take much longer from the test to the marketplace.

Bibliography

[1] J.S.E.M. Svensson, and C.G. Granqvist, *Solar Energy Materials,* 12 (1985) 391.

[2] J.S.E.M. Svensson, and C.G. Granqvist, *Thin Solid Film,* 126 (1985) 31.

[3] J.S.E.M. Svensson, and C.G. Granqvist, *Appl. Phys. Lett.,* 45 (1984) 828.

[4] T. Kamimori, J. Nagai and M. Mizuhashi, *Solar Energy Materials,* 16 (1987) 27.

[5] C. M. Lampert, *Solar Energy Materials,* 11 (1984) 1.

[6] K. Miyake, H. Kaneko, M. Sano and N. Suedomi, *J. Appl. Phys.,* 55 (1984) 2747.

[7] P. Gerard, A. Deneuville and R. Courths, *Thin Solid Films,* 71 (1980) 221.

[8] S. K. Deb, *Philos. Mag.,* 27 (1973) 801.

[9] H. Kaneko, S. Nishimoto, K. Miyake and N. Suedomi, *J. Appl. Phys.,* 59 (1986) 2526.

[10] S. F. Cogan, T. D. Plante, M. A. Parker and R. D. Rauh, *J. Appl. Phys.,* 60 (1986) 2735.

[11] H. Kaneko, K. Miyake and Y. Teramoto, *J. Apppl. Phys.,* 53 (1982) 4416.

[12] R. B. Goldner, D. H. Mendelsohn, J. Alexander, W. R. Henderson, D. Fitzpatrick, T. E. Haas, H. H. Sample, R. D. Rauh, M. A. Parker and T. L. Rose, *Appl. Phys. Lett.,* 43 (1983) 1093.

[13] D. Davazoglau and A. Donnadieu, *Solar Energy Materials,* 16 (1987) 55.

[14] D. Craigen, A. Mackintosh, J. Hickman and K. Colbow, *J. Electrochem. Soc.,* 133 (1986) 1529.

[15] O. F Schirmer, V. Wittwer, G. Baur and G. Brandt, *J. Electrochem. Soc.,* 124 (1977) 749.

[16] A. Nakamura, *Appl. Phys.*, 24 (1981) 55.

[17] H. R. Zeller and H. U. Beyeler, *Appl. Phys.*, 13 (1977) 231.

[18] S. Tanisaki, *Journal of the Physical Society of Japan*, 15 (1960) 566.

[19] E. Salje and K. Viswanathan, *Acta Cryst.*, A31 (1975) 356.

[20] E. Salje, *Acta Cryst.*, B33 (1977) 574.

[21] J. V. Gabrusenoks, P. D. Cikmach, A. R. Lusis, J. J. Kleperis and G. M. Ramans, *Solid State Ionics*, 14 (1984) 25.

[22] A. P. Schuster, D. Nguyen and O. Caporaletti, *Solar Energy Materials*, 13 (1986) 153.

[23] D. W. Bullett, *J. Phys. C: Solid State Phys.*, 16 (1983) 2197.

[24] H. N. Hersh, W. E. Kramer and J. H. Mcgee, *Appl. Phys. Lett.*, 27 (1975) 646.

[25] R. S. Crandall and B. W. Faughnan, *Appl. Phys. Lett.*, 26 (1975) 120.

[26] I. F. Chang, B. L. Gilbert and T. I. Sun, *J. Electrochem. Soc.*, 122 (1975) 955.

[27] R. Hurditch, *Electron Lett.*, 11 (1975) 142.

[28] B. W. Faughnan and R. S. Crandall, and P. M. Heyman, *RCA Review*, 36 (1975) 177.

[29] B. W. Faughnan and R. S. Crandall, *Appl. Phys. Lett.*, 31 (1977) 834.

[30] T. Nishimura, K. Taira and S. Kurita, *Appl. Phys. Lett.*, 36 (1980) 585.

[31] H. Muramatsu, T. Itoh, A. Watanabe and K. Hara, *Japanese Journal of Applied Physics*, 21 (1982) L73.

[32] A. Deneuville, P. Gerard and R. Billat, *Thin Solid Films*, 70 (1980) 203.

[33] J. H. Pifer and E. K. Sichel, *Journal of Electronic Materials*, 9 (1980) 129.

[34] B. Ampe, J. M. Leroy, D. Thomas and G. Tridot, *Revue de Chimie minerale*, 5 (1968) 801.

[35] P. G. Dickens and R. J. Hurditch, *Nature,* 215 (1967) 1267.

[36] B. S. Hobbs and A. C. C. Tseung, *J. Electrochem. Soc.*, 119 (1972) 580.

[37] P. J. Wiseman and P. G. Dickens, *Journal of Solid State Chemistry,* 6 (1973) 374.

[38] S. K. Mohapatra, *J. Electrochem. Soc.*, 125 (1978) 284.

[39] J. Nagai and T. Kamimori, *Japanese Journal of Applied Physics,* 22 (1983) 681.

[40] M. Campagna, G. K. Wertheim, H. R. Shanks, F. Zumsteg and E. Banks, *Physical Review Letters,* 34 (1975) 738.

[41] J. F. Owen, K. J. Teegarden and H. R. Shanks, *Physical Review B,* 18 (1978) 3827.

[42] R. B. Goldner, K. Wong, G. Foley, P. Norton, L. Wamboldt, G. Seward, T. Haas and R. Chapman, *Solar Energy Materials,* 16 (1987) 365.

[43] R. B. Goldner, *Solar Energy Materials,* 11 (1984) 177.

[44] D. H. Mendelsohn and R. B. Goldner, *J. Electrochem. Soc.*, 131 (1984) 857.

[45] L. J. van der Pauw, *Philips Technical Review,* 20 (1959) 220.

[46] J. Lange, *Journal of Applied Physics,* 35 (1961) 2659.

[47] K. L. Chopra and S. K. Bahl, *J. Appl. Phys.*, 38 (1967) 3607.

[48] E. W. Nuffield, *X-ray Diffraction Methods*, John Wiley and Sons, New York, (1966).

[49] L. I. Mirkin, *Handbook of X-ray Analysis of Polycrystalline Materials,* Consultants Bureau, New York, (1964).

[50] G. Zhou, S. Wessel, and K. Colbow, *J. Phys. D: Appl. Phys.*, 21 (1988) 1802.

[51] M. Fantini, I. L. Torriani and C. Constantino, *Journal of Crystal Growth,* 74 (1986) 439.

[52] G. Zhou, *Pyrolytically Spray Deposited Electrochromic WO_3 Films*, M.sc. Thesis, S. F. U., Canada, (1987).

[53] G. Beni, *Solid State Ionics*, 3/4 (1981) 157.

[54] J. P. Randin and R. Viennet, *J. Electrochem. Soc.*, 129 (1982) 2349.

[55] R. S. Crandall and B. W. Faughnan, *Physical Review Letters*, 39 (1977) 232.

[56] M. L. Hitchman, *Thin Solid Films*, 61 (1979) 341.

[57] A. I. Gavrilyuk, V. G. Prokhvatilov and F. A. Chudnovskil, *Sov. Phys. Solid State*, 24 (1982) 558.

[58] R. B. Goldner, A. Brofos, G. Foley, E. L. Goldner, T. E. Haas, W. Henderson, P. Norton, B. A. Ratnam, N. Weis and K. K. Wong, *Solar Energy Materials*, 12 (1985) 403.

[59] R. B. Golder, P. Norton, K. Wong, G. Foley, E. L. Goldner, G. Seward and R. Chapman, *Appl. Phys. Lett.*, 47 (1985) 536.

[60] I. Hamberg and C. G. Granqvist, *Appl. Phys. Lett.*, 44 (1984) 721.

[61] F. Wooten, *Optical Properties of Solids*, Academic Press, New York and London, (1972).

[62] E. Gerlach and P. Grosse, *Festkorperprobleme* XVII (1977) 157.

[63] C. Kittel, *Introduction to Solid State Physics*, 5th ed., Wiley, New York, (1976).

[64] H. Haitjema and J. Elich, *Solar Energy Materials*, 16 (1987) 79.

[65] F. Simonis, A. J. Faber and C. J. Hoogendoorn, *Journal of Solar Energy Engineering*, 109 (1987) 22.

[66] B. Moore, *Popular Science*, December (1987) 68.